

AD-A073 395

NAVAL POSTGRADUATE SCHOOL MONTEREY CA

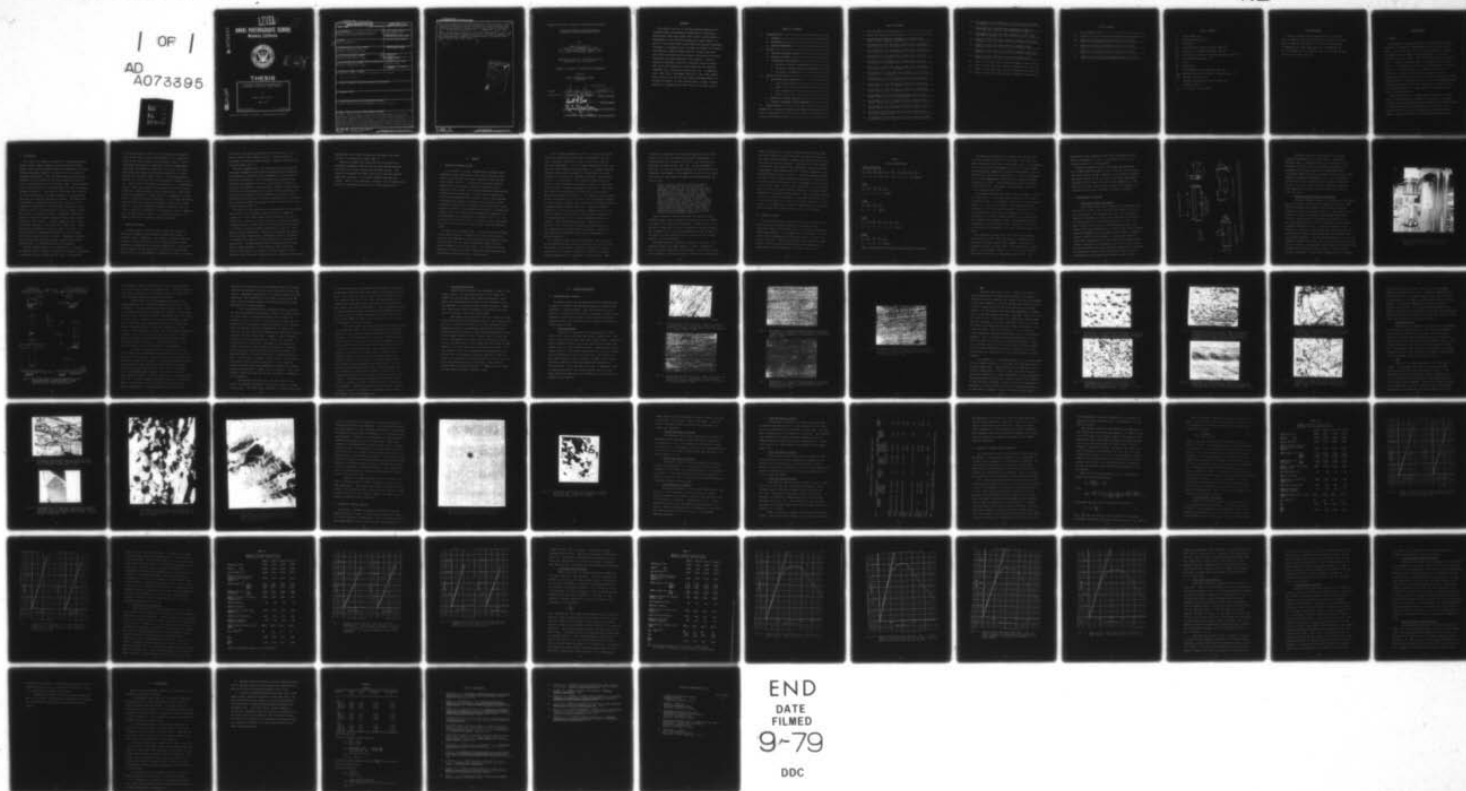
F/G 11/6

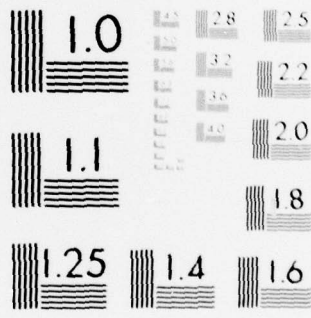
FRACTURE TOUGHNESS CHARACTERIZATION OF SELECTED ULTRA HIGH CARB--ETC(U)  
JUN 79 J L TAYLOR

UNCLASSIFIED

NL

| OF |  
AD  
A073395





MICROCOPY RESOLUTION TEST CHART  
NATIONAL BUREAU OF STANDARDS-1963-A

LEVEL *11*

②

AD A 073395

# NAVAL POSTGRADUATE SCHOOL

Monterey, California



DDC  
RACILAE  
SEP 4, 1979  
R  
C

## THESIS

FRACTURE TOUGHNESS CHARACTERIZATION  
OF SELECTED ULTRA HIGH CARBON STEELS

by

James Louis Taylor

June 1979

Thesis Advisor:

T. R. McNelley

DDC FILE COPY

Approved for public release; distribution unlimited

79 08 31

UNCLASSIFIED

SECURITY CLASSIFICATION OF THIS PAGE (When Data Entered)

REPORT DOCUMENTATION PAGE		READ INSTRUCTIONS BEFORE COMPLETING FORM
1. REPORT NUMBER	2. GOVT ACCESSION NO.	3. RECIPIENT'S CATALOG NUMBER
4. TITLE (and Subtitle) Fracture Toughness Characterization of Selected Ultra High Carbon Steels		5. TYPE OF REPORT & PERIOD COVERED Master's Thesis June 1979
7. AUTHOR(s) James Louis/Taylor		6. PERFORMING ORG. REPORT NUMBER
8. PERFORMING ORGANIZATION NAME AND ADDRESS Naval Postgraduate School Monterey, California 93940		9. CONTRACT OR GRANT NUMBER(s)
11. CONTROLLING OFFICE NAME AND ADDRESS Naval Postgraduate School Monterey, California 93940		10. PROGRAM ELEMENT, PROJECT, TASK AREA & WORK UNIT NUMBERS
14. MONITORING AGENCY NAME & ADDRESS (if different from Controlling Office) Naval Postgraduate School Monterey, California 93940		12. REPORT DATE June 1979
		13. NUMBER OF PAGES 74 pages
		15. SECURITY CLASS. (of this report) Unclassified
		16a. DECLASSIFICATION/DOWNGRADING SCHEDULE
14. DISTRIBUTION STATEMENT (of this Report) Approved for public release; distribution unlimited.		
17. DISTRIBUTION STATEMENT (of the abstract entered in Block 20, if different from Report)		
18. SUPPLEMENTARY NOTES		
19. KEY WORDS (Continue on reverse side if necessary and identify by block number) Ultra high carbon steels, fracture toughness testing		
20. ABSTRACT (Continue on reverse side if necessary and identify by block number) This effort, part of an ongoing program examining the micro-structural and mechanical properties of extensively warm-worked ultra high carbon (UHC) steels, was directed at measurement of the fracture toughness of these steels. A facility was constructed to test bend-type fracture toughness specimens in accordance with the American Society for Testing and Materials (ASTM) Standard E399-78; several UHC steel alloys were evaluated and the results correlated		

UNCLASSIFIED

SECURITY CLASSIFICATION OF THIS PAGE (When Data Entered)

with microstructural and other mechanical test results. With one exception, processing failed to eliminate coarse carbides from the microstructures of these materials and fracture toughness,  $K_{IC}$ , values were accordingly low. A commercial alloy, AISI 52100, processed similarly to the other experimental alloys, did not have the coarse carbides present to as great an extent, and was significantly tougher, as manifested by a strength ratio twice that of the other alloys.

(IC)

A

Accession For	
NTIS GRA&I	
DDC TAB	
Unannounced	
Justification	
By	
Distribution/	
Availability Codes	
Dist	Availand/or special
A	

UNCLASSIFIED

SECURITY CLASSIFICATION OF THIS PAGE (When Data Entered)

Approved for public release; distribution unlimited

Fracture Toughness Characterization  
of Selected Ultra High Carbon Steels

by

James Louis Taylor  
Lieutenant Commander, U.S. Navy  
B.S., United States Naval Academy, 1965  
M.S., Naval Postgraduate School, 1977

Submitted in partial fulfillment of the  
requirements for the degree of

MASTER OF SCIENCE IN MECHANICAL ENGINEERING

from the

NAVAL POSTGRADUATE SCHOOL  
June 1979

Author

James L. Taylor

Approved by:

Gerry R. McElroy  
Thesis Advisor

Donald F. Gooe  
Second Reader

R. E. Newton  
Chairman, Department of Mechanical Engineering

William M. Solles  
Dean of Science and Engineering

## ABSTRACT

This effort, part of an ongoing program examining the microstructural and mechanical properties of extensively warm-worked ultra high carbon (UHC) steels, was directed at measurement of the fracture toughness of these steels. A facility was constructed to test bend-type fracture toughness specimens in accordance with the American Society for Testing and Materials (ASTM) Standard E399-78; several UHC steel alloys were evaluated and the results correlated with microstructural and other mechanical test results. With one exception, processing failed to eliminate coarse carbides from the microstructures of these materials and fracture toughness,  $K_{IC}$ , values were accordingly low. A commercial alloy, AISI 52100, processed similarly to the other experimental alloys, did not have the coarse carbides present to as great an extent, and was significantly tougher, as manifested by a strength ratio twice that of the other alloys.

TABLE OF CONTENTS

I. INTRODUCTION----- 11

    A. PURPOSE----- 11

    B. BACKGROUND----- 12

    C. PREVIOUS RESEARCH----- 13

II. REVIEW----- 16

    A. FRACTURE TOUGHNESS THEORY----- 16

    B. MATERIAL HISTORY----- 19

    C. EXPERIMENTAL PROCEDURES----- 22

        1. Mechanical Testing Procedures----- 22

        2. Fracture Toughness Testing Procedures----- 24

        3. Microscopy Procedures----- 30

III. RESULTS/DISCUSSION----- 31

    A. MICROSTRUCTURAL ANALYSIS----- 31

        1. Light Microscope----- 31

        2. SEM----- 35

        3. Macro Examination----- 39

        4. TEM----- 39

    B. MECHANICAL TESTING RESULTS----- 43

    C. FRACTURE TOUGHNESS TESTING RESULTS----- 49

IV. CONCLUSIONS----- 69

APPENDIX A: Specimen Dimensions and Sample Calculations--- 71

List of References----- 72

Initial Distribution List----- 74

## LIST OF FIGURES

1.	Test specimen specifications-----	23
2.	Series 810 materials test system-----	25
3.	Top and bottom mounting assemblies for three point bend fracture toughness specimen-----	26
4.	Micrograph of 52150 UHC steel etched with a saturated picral solution for one minute-----	32
5.	Micrograph of 53150 UHC steel etched with a saturated picral solution for 30 seconds-----	32
6.	Micrograph of 43150 UHC steel etched with a 2% nital solution for 20 seconds-----	33
7.	Micrograph of 10150 UHC steel etched with a 2% nital solution for 20 seconds-----	33
8.	Micrograph of 52100 UHC steel etched with a saturated picral solution for 25 seconds-----	34
9.	Micrograph of a 10150 UHC steel etched with a 2% nital solution for 20 seconds-----	36
10.	Micrograph of 52100 UHC steel etched with a saturated picral solution for 25 seconds-----	36
11.	Micrograph of 52150 UHC steel etched with a saturated picral solution for 25 seconds-----	37
12.	Micrograph of 52150 UHC steel etched with a saturated picral solution for 25 seconds-----	37
13.	Micrograph of 52150 UHC steel fracture surface after a Charpy Impact Test at room temperature-----	38
14.	Micrograph of 52150 UHC steel fracture surface after a Charpy Impact Test at 100°C-----	38
15.	Micrograph of 52150 UHC steel fracture surface after a Charpy Impact Test at 220°C-----	40
16.	Micrograph of 52150 UHC steel fracture surface after a fracture toughness test-----	40
17.	Micrograph of 10150 UHC steel as rolled taken with TEM at 10000X with a 6° tilt-----	41

18.	Micrograph of 10150 UHC steel as rolled taken with TEM at 20000X-----	42
19.	Micrograph of a selected area defraction pattern of 10150 UHC steel with one second exposure on TEM-----	44
20.	Micrograph of 10150 UHC steel annealed at 650 <sup>o</sup> C taken with TEM at 20000X-----	45
21.	Graphs of 53150 UHC steel fracture toughness tests one and two-----	53
22.	Graphs of 53150 UHC steel fracture toughness tests three and four-----	54
23.	Graphs of 43150 UHC steel fracture toughness tests one and two-----	57
24.	Graphs of 43150 UHC steel fracture toughness tests three and four-----	58
25.	Graph of 52100 UHC steel fracture toughness test one---	61
26.	Graph of 52100 UHC steel fracture toughness test two---	62
27.	Graph of 52100 UHC steel fracture toughness test three-	63
28.	Graph of 52100 UHC steel fracture toughness test four--	64

## LIST OF TABLES

I.	Alloy Compositions-----	20
II.	Properties of Tested Ultra High Carbon Steel Alloys---	48
III.	Results of Fracture Toughness Tests for 53150 UHC Steel Alloy as Rolled-----	52
IV.	Results of Fracture Toughness Tests for 43150 UHC Steel Alloy as Rolled-----	56
V.	Results of Fracture Toughness Tests for 52100 UHC Steel Alloy as Rolled-----	60
VI.	Dimensions of Fracture Toughness Specimens for 53150, 43150 and 52100 UHC Steel Alloys-----	71

## LIST OF SYMBOLS

a	crack length (cm)
B	specimen thickness (cm)
cm	centimeter
$K_f$	fatigue stress intensity factor ( $\text{MPa}\cdot\text{m}^{1/2}$ )
$K_{IC}$	plane-strain fracture toughness ( $\text{MPa}\cdot\text{m}^{1/2}$ )
$K_Q$	conditional (apparent) fracture toughness ( $\text{MPa}\cdot\text{m}^{1/2}$ )
KSI	kilo-pounds per square inch
m	meter
MPa	megapascals
$P_Q$	load determined from secant method (KN)
$P_{\max}$	maximum load during fracture toughness test (KN)
$R_{sb}$	specimen strength ratio
S	specimen span between roller notches (cm)
W	specimen width (cm)
$\sigma_{YS}$	0.2% offset yield strength

#### ACKNOWLEDGMENT

I wish to express my deep appreciation to Professor Terry R. McNelley for the many hours of guidance and assistance he gave me, Professor G. H. Lindsey and Professor T. Yamashita for their assistance, Mr. Tom Kellogg and Mr. Ken Graham for their support, and Chris, Susan, Richard and Heidi for their patience.

## I. INTRODUCTION

### A. PURPOSE

The purpose of this research was to determine the fracture toughness of extensively warm-worked ultra high carbon (UHC) steels. This effort was part of ongoing research at the Naval Postgraduate School (NPS) into the mechanical and ballistic properties of these steels. This work follows that of Goesling [Ref. 1], Hamilton and Rowe [Ref. 2] and Martin and Phillips [Ref. 3], who emphasized the ballistic characteristics of these materials. One major goal of this work was to develop the capability at NPS to conduct fracture toughness testing in accordance with American Society for Testing and Materials (ASTM) Standard E399-78, contained in Ref. 4. Various thermomechanically processed UHC steel alloys were examined to evaluate alloying and processing effects on these materials' resistance to unstable crack propagation.

The ultimate goal of the NPS research effort is to understand the microstructural, mechanical, processing and compositional variables which govern the toughness of these UHC steels. It is believed that this understanding will assist in the eventual use of UHC steel in important applications such as armor in military vehicles and as improved bearing material.

## B. BACKGROUND

UHC steels are normally classified as those steels whose carbon content ranges between one and two weight percent. Higher carbon contents improve both the hardenability and the maximum attainable hardness of steels, but at the price of increased brittleness. Such brittleness may result from the formation of iron carbide at the grain boundaries when the steel is slow-cooled from the austenite range. These carbides are brittle and provide a preferred path for crack propagation through the material. The nature of UHC steels has resulted in their limited use in industry, primarily in applications requiring high hardness and wear resistance. UHC steels may be hardened by quenching from austenite, resulting in the formation of martensite, a body centered tetragonal crystal structure which is very hard due to the high carbon content, but, again, is relatively brittle. Subsequent tempering is normally required to enhance toughness and relieve residual stresses in this material. Several commercial tool steels have carbon contents in the ultra high carbon range. These materials are frequently alloyed in such a way that it is often difficult to adequately dissolve all of the carbon during the austenitizing of the steel. Subsequent quenching then retains some relatively coarse, undissolved carbides, leading, again, to reduced ductility and toughness.

The NPS research effort is an outgrowth of a discovery by Professor Oleg D. Sherby, of Stanford University's Department of Material Science and Engineering, that, by extensively

rolling UHC steels as they are cooled through the austenite plus carbide region of the phase diagram, it is possible to break up the grain boundary carbide network [Refs. 2 and 3]. Isothermal warm-working of these UHC steels at temperatures just below the eutectoid temperature can result in a fine, particulate and spheroidal carbide distribution in a fine-grained ferrite matrix [Refs. 1 and 7]. This microstructure results in a steel with both high strength and improved ductility. These steels also exhibit superplasticity at temperatures slightly below the eutectoid, which means they can be readily formed into complex shapes at these temperatures. When these steels are subsequently austenitized at a temperature slightly above the eutectoid and then quenched, a fine grained martensite and fine spheroidal carbide two-phased microstructure results [Ref. 5]. This microstructure suggests a material which has a high resistance to unstable crack propagation which, combined with its high strength, makes it an attractive material for numerous applications requiring these attributes.

#### C. PREVIOUS RESEARCH

The NPS research effort into UHC steels was started by Lieutenant Commander William Goesling under the guidance of Professor Terry R. McNelley. The interest in these steels was centered on their potential use as an armor material, where hardness and toughness are the prime requirements. This initial effort resulted in the fabrication of the NPS Ballistic Test Facility and the establishment of procedures for data collection.

The initial test results indicated that 52100 steel (a one percent carbon steel commonly used as a bearing material), processed following the Sherby method, compared favorably with existing armors [Ref. 1].

Ballistic examination of the 52100 steel was continued by Lieutenant Commander Donald Rowe and Captain Douglas Hamilton who examined the effects of heat treatment on this material's ballistic performance. They determined that austenitizing, quenching and tempering this steel significantly reduced its ballistic performance. Microstructural examination determined that there was considerable grain growth during austenitizing and that the subsequent quench produced a relatively coarse martensite which was less resistant to penetration by relatively soft fragment simulating projectiles than the same steel in the rolled condition [Ref. 2].

The scope of the research effort was broadened by Lieutenant Ronald Martin and Lieutenant James Phillips who commenced studies on a 1.67% carbon steel while continuing the study of 52100 steel. Special attention was given to the metallographic characterization of these steels after they were penetrated by .22 caliber, 17-grain fragment simulating projectiles. Both materials were subjected to various rolling conditions and the 52100 steel was given several subsequent annealing treatments to determine the effects of these processes on resistance to penetration. It was determined that "warm-worked UHC steels have a lesser tendency to form adiabatic shear bands than several conventional steel armors." These adiabatic shear bands are associated with reduced ballistic penetration resistance.

Warm-worked 52100 steel's ballistic performance was found superior to conventional armors [Ref. 3].

Ballistic research has continued with the efforts of Lieutenant Commander Randy Hillier who has further expanded the effort to include various new UHC steel alloys. The effects of chromium and nickel alloying on ballistic performance were examined. A 1.5% plain carbon steel was also tested. None of these materials, however, has yet demonstrated ballistic performance as good as the 52100 steel [Ref. 8].

## II. REVIEW

### A. FRACTURE TOUGHNESS THEORY

A. A. Griffith, in 1920, proposed that unstable crack propagation would take place if the elastic strain energy release rate exceeded the energy required to form the new crack surface [Ref. 9]. In studies with glass, Griffith demonstrated a functional relationship between failure stress and crack length. The theory worked well when applied to materials which behaved in a purely elastic manner but the problem became much more difficult when it was necessary to evaluate the energies involved in the process of crack propagation when plastic deformation took place before crack extension occurred. This focused the attention of researchers "toward crack tip characterizing parameters as measurers of the susceptibility of materials to fracture" [Ref. 10]. The original work of Griffith [Ref. 9], however, still represents the basis for the field of linear elastic fracture mechanics (LEFM).

In 1948, Irwin proposed [Ref. 11] that the Griffith energy balance must actually be between the elastic strain energy stored in the specimen on one hand and the free surface energy plus the work done in plastic deformation associated with crack propagation on the other hand. For relatively ductile materials, the work of plastic deformation would dominate the free-surface energy and make it insignificant.

In 1955, Orowan demonstrated [Ref. 12] that the Griffith condition, when modified for plastic deformation, was not only a necessary condition but was a sufficient condition for crack propagation. In 1957, Irwin demonstrated [Ref. 13] that the energy approach was equivalent to a stress-intensity approach, where crack propagation occurred when the stress intensity at the crack tip reached a critical value characteristic of the material. This concept spurred efforts to develop a test specimen and procedure suitable for measuring the plane strain fracture toughness of materials. The theory was limited to those materials which have limited plastic deformation around the crack tip. "If extensive plastic deformation takes place prior to failure, the relationship between an energy balance approach and a crack tip environment approach becomes much more tenuous" [Ref. 10]. Tests on numerous specimens of varying size and material demonstrated that the stress intensity at the crack tip was strongly dependent on the plate thickness until a certain minimum thickness was reached. This minimum thickness was a function of the material. Only after this thickness was exceeded did the test results give a constant stress intensity, indicating that this stress intensity value could be considered a material property.

The thickness effect on crack propagation was explained by the observation that plastic regions at the crack tip near the surface of the material approach a condition of plane stress, while the plastic regions at the crack tip remote from the surface are in a condition of plane strain. "When

thickness is sufficient, the fracture behavior will be dominated by the region of constrained plastic deformation, a characteristic flat fracture will occur, and conditions are described as plane strain. [Ref. 14]. It was observed by Liu [Ref. 15] that the fracture behavior is controlled by the mechanical environment in the immediate vicinity of the crack tip and not by the elastic stresses and strains outside the plastic zone.

Within a certain radius the stress intensity factor characterizes the stress field and, provided the plastic zone is sufficiently small compared to this radius, the elastic field will be unaffected by plastic relaxation. Thus, for two different situations, say two different geometries, where the same stress intensity factor is applied, conditions of stress, strain, etc., at geometrically similar points will be identical even within the plastic zone, provided these zones are much smaller than the radius at which conditions may be considered as specified by the stress intensity factor. Under these restrictions the fracture event will be characterized by the attainment of  $K_{IC}$ , the critical value of stress intensity [Ref. 14].

Stress intensity factors have been determined for many geometries and loading conditions through the use of a number of numerical and analytical techniques. These results can be applied to laboratory tests to investigate fracture toughness. The determination of  $K_{IC}$  through testing can then be used in the design of real structures and in predicting the fracture behavior of real structures.

The LEFM approach is severely limited in that only a few materials exhibit the small amount of plastic deformation prior to failure required by the approach. It was anticipated that, because of the high strength of UHC steels, these steels

might be suitable for fracture toughness testing using LEFM. Alternate methods have been developed for materials exhibiting elastic-plastic behavior whereby the plastic region around the crack tip is more extensive. Research into these methods is continuing and presently two approaches, the Crack Opening Displacement (COD) Approach and the J-Integral Approach, show the most promise [Refs. 16 and 17]. The COD approach attempts to deal with the plastic deformation by making a correction to the crack length by measuring the displacement across the face of the crack. There is still much uncertainty in this approach but it provides the best present alternative for testing when materials do not exhibit LEFM behavior. The J-Integral Approach uses J as a crack tip parameter in nonlinear elasticity, but it is not yet clear if it can be used under conditions of plasticity. It is calculated in much the same manner as COD except the area under the load-displacement curve is evaluated.

#### B. MATERIAL HISTORY

The various UHC steel alloys tested for this research were received from the Research Laboratory of Republic Steel Corporation where they had been cast in the form of cylindrical ingots approximately 7.6 cm diameter by 23 cm length. In this section the thermomechanical processing history of each alloy will be recalled. Table I provides the alloy content of these steels. The processing described below was accomplished at Viking Metallurgical Corporation in Albany, California.

Table I

## ALLOY COMPOSITIONS

52150-1 and 52150-2

C	Si	Cr	Mn	P	Al	Cu	Mo	Ni	Fe
wt %	wt %	wt %	wt %	wt %	wt %				
1.47	0.1	1.28	0.66	0.013	0.015	0.02	0.01	0.04	Balance

53150

C	Si	Cr	Mn	Fe
wt %				
1.5	0.1	2.25	0.5	Balance

10150

C	Si	Mn	Fe
wt %	wt %	wt %	wt %
1.5	0.1	0.5	Balance

43150

C	Si	Cr	Mn	Mo	Ni	Fe
wt %						
1.5	0.1	1.0	0.5	0.25	1.5	Balance

52100

C	Si	Cr	Mn	Fe
wt %				
1.0	0.19	1.35	0.32	Balance

NOTE: Weight percents represent maximum amounts presented.

The materials denoted 52150, batches one and two, were solution treated at 1150°C for five hours. They were then upset forged at 1150°C from a cylindrical ingot 7.6 cm diameter x 23 cm to a billet approximately 12.7 cm x 7.6 cm x length. The specimen was immediately rolled at approximately 0.09 cm reduction per pass from a thickness of 7.6 cm to a thickness of 2.5 cm as temperature cooled from the forging finishing temperature to 650°C. The specimens were then isothermally rolled at 650°C to a thickness of approximately 0.64 cm at 0.08 cm reduction per pass.

The material denoted 53150 was solution treated at 1175°C for eight hours. It was then upset forged at 1175°C from a cylindrical ingot 7.6 cm diameter x 23 cm to a billet approximately 12.7 cm x 7.6 cm x length. The specimen was then reheated to 1175°C for about two hours. Starting at 1175°C, the specimen was rolled from a thickness of 7.6 cm to a thickness of 2.5 cm at a reduction rate of 0.09 cm per pass while temperature dropped to 650°C. The specimen was then isothermally rolled at 650°C from a thickness of 2.5 cm to a thickness of approximately 0.64 cm at 0.08 cm reduction per pass.

The materials denoted 43150 and 10150 were processed identically to 53150. The 52100 steel, a commercial steel obtained from Vasco Pacific Steel Company, was solution treated at 1000°C for three hours. The specimen was forged from a 7.9 cm diameter round to a 7.6 cm x 5.1 cm x length plate and air cooled to a temperature below 300°C. The

specimen was then reheated to 650°C and isothermally rolled from a thickness of 5.1 cm to a thickness of 0.64 cm at a reduction rate of 0.13 cm per pass.

Fracture toughness, tensile and Charpy specimens were cut to specifications shown in Fig. 1 from the various alloys upon their receipt at NPS. Several of the fracture toughness specimens from the 53150 and 10150 alloys were subsequently annealed at 650°C and air cooled to room temperature at NPS. Testing after such annealing was conducted to determine the influence of this heat treatment on fracture toughness.

### C. EXPERIMENTAL PROCEDURES

#### 1. Mechanical Testing Procedures

Sheet type tensile test specimens were machined from the 52150-1, 52150-2, 53150 and 43150 UHC steels in the as-rolled condition. One specimen was cut in the transverse direction (transverse to the rolling direction) from each of the above steels to the specifications given in Fig. 1.C. Gage lengths for all tensile test specimens were one inch. Tensile tests were conducted on an Instron Model TT-D Universal Testing Instrument utilizing wedge action grips to eliminate nonaxial loading of the specimen. Load-versus-elongation curves were autographically recorded while the specimens were loaded to failure at an extension rate of 0.13 cm per minute. The data obtained from these tests were subsequently converted to engineering stress versus engineering plastic strain to determine the yield stress and ultimate tensile stress.

TEST SPECIMEN SPECIFICATION

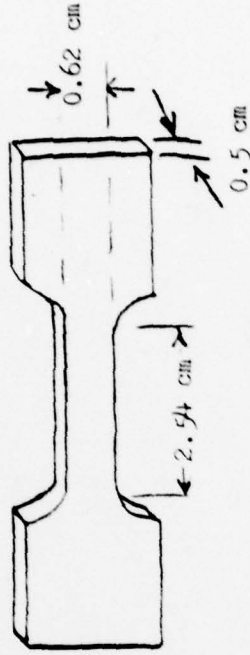
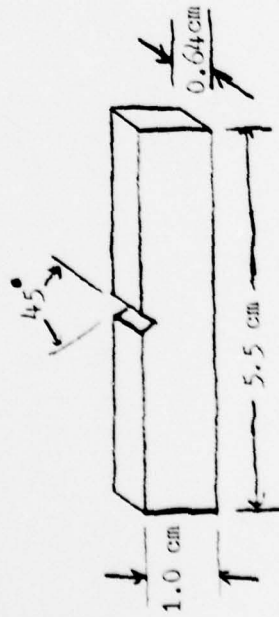
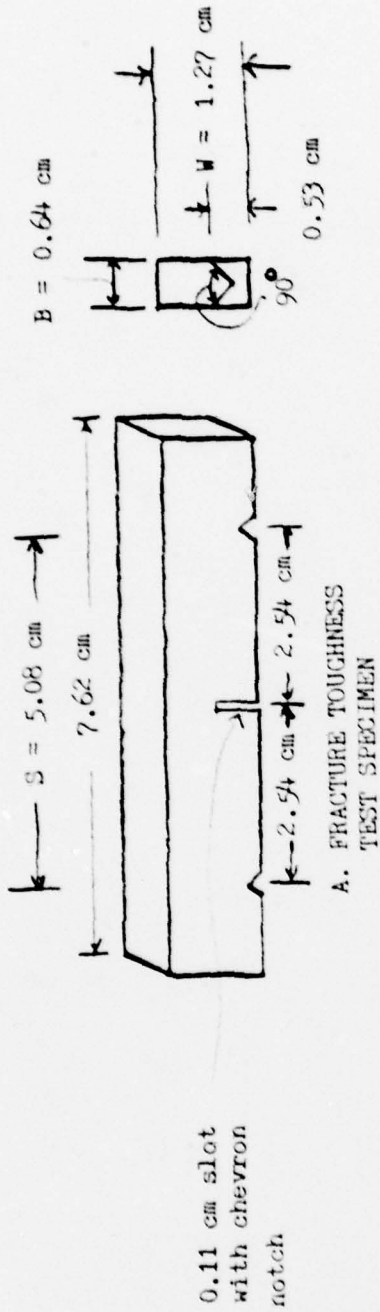


Fig. 1. Test specimen specifications. These drawings depict the dimensions of the UHC steel specimens used in fracture toughness (A), impact (B) and tensile (C) tests.

Hardness testing was conducted on the fracture toughness specimens using a Wilson Model 1 JR Rockwell Hardness Tester. Hardness results were determined by disregarding the first value and averaging a minimum of six subsequent test values obtained on a machined surface. Notched-bar impact testing was conducted utilizing the Charpy method on specimens as depicted in Fig. 1.B. to determine the amount of energy absorbed when a notched specimen was broken. All alloys except 10150 UHC steel were tested at room temperature and 52150 UHC steel was also tested at 100°C and 220°C.

## 2. Fracture Toughness Testing Procedures

Fracture toughness testing on a three-point bend specimen was conducted following the procedures outlined in ASTM E399-78, Standard Test Method for Plane Strain Fracture Toughness of Metallic Materials [Ref. 4]. The tests were conducted on a Series 810 Materials Test System (MTS) Model 976.01-31 servo-hydraulic test machine pictured in Fig. 2. The test specimen in Fig. 1.A was positioned on the loading apparatus described in Fig. 3. One of the goals of this effort was to design a test fixture which would minimize the errors arising from friction between the test specimen and the loading apparatus. This was accomplished by using 0.32 cm diameter hardened steel dowel pins as rollers which fitted into the two notches on the specimen bottom face and provided rolling contact with the bottom loading fixture. The top loading fixture contained a 0.48 cm radius hardened steel pin welded

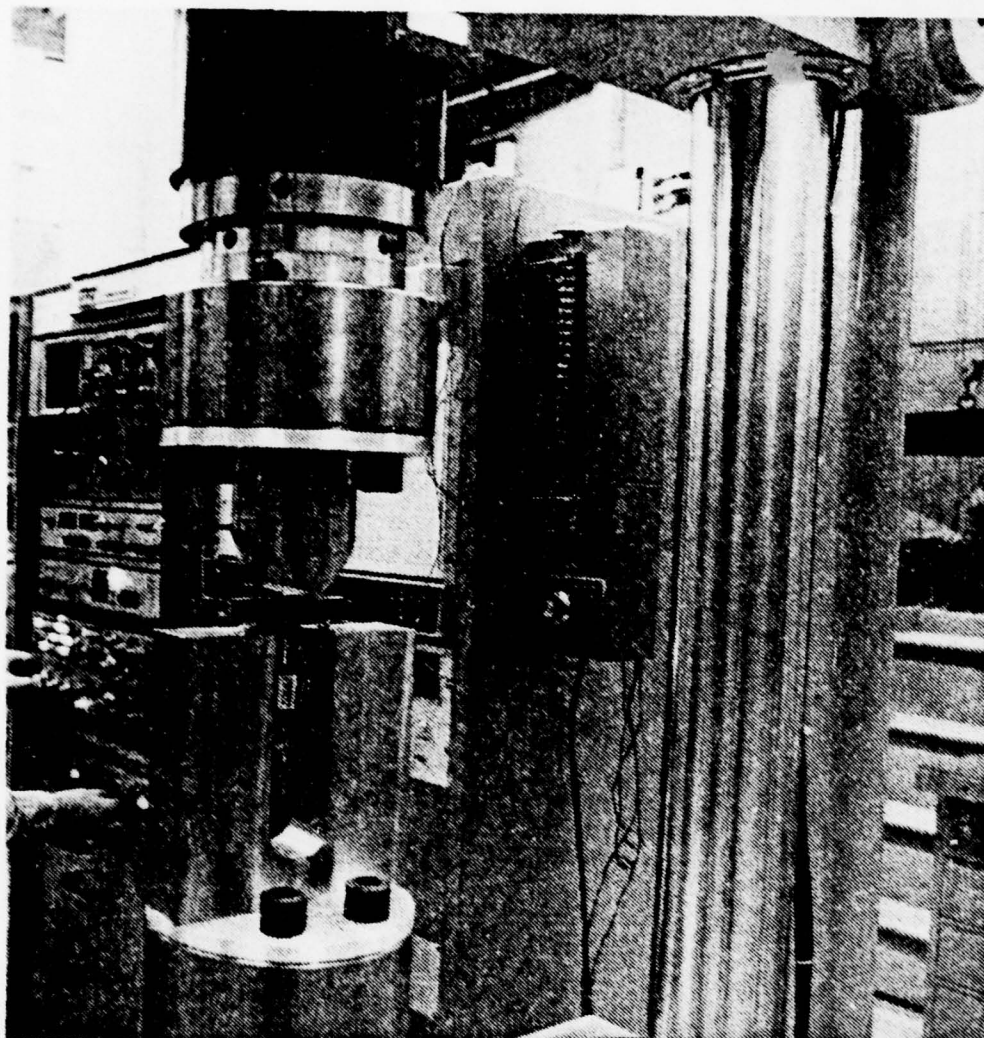


Fig. 2: Series 810 Materials Testing System and associated loading apparatus. Fracture toughness specimen is mounted with clip gage monitoring crack opening displacement.

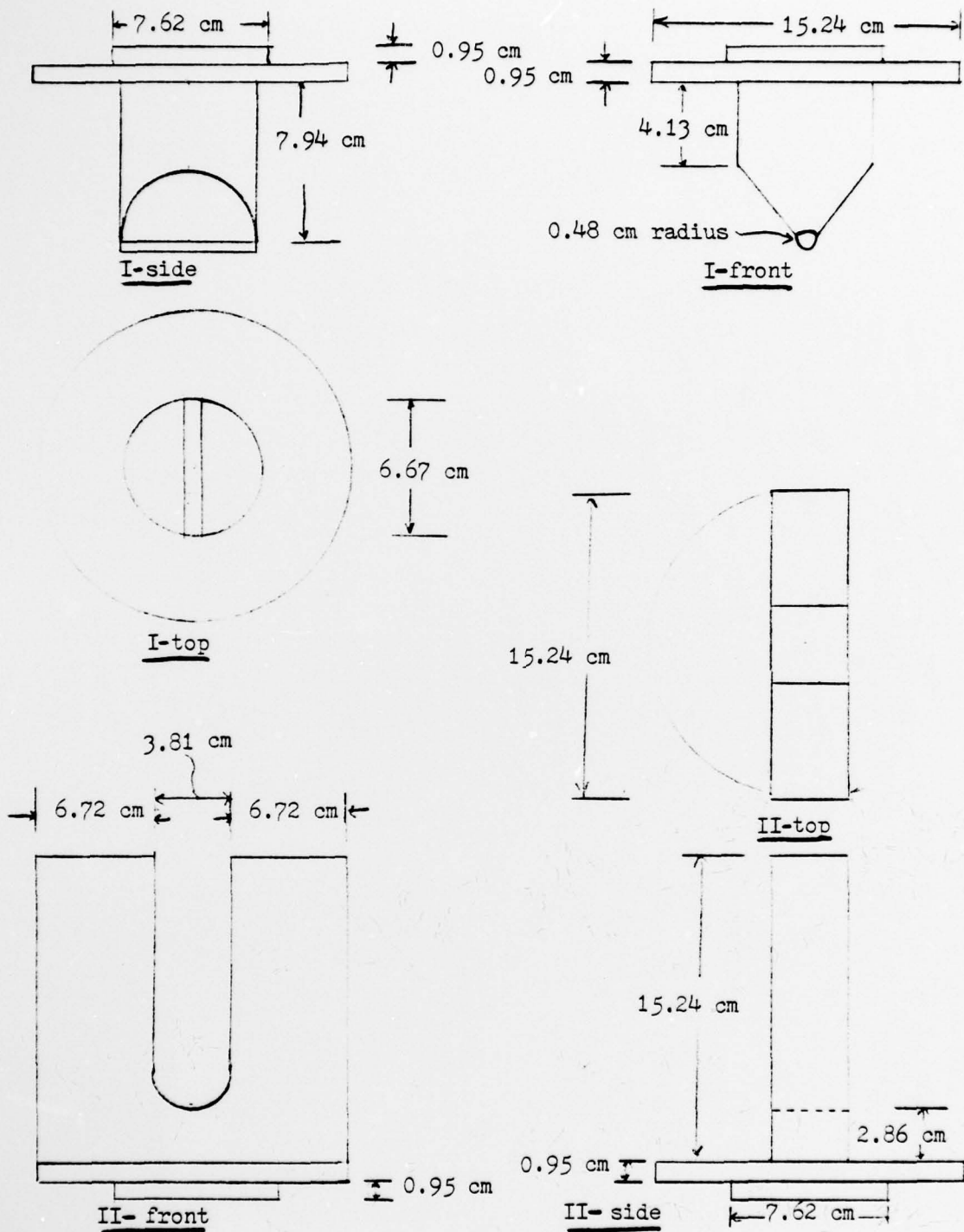


Fig. 3: Top (I) and bottom (II) mounting assemblies for three point bend fracture toughness specimen. Assembly manufactured from a medium strength steel.

to the upper fixture, which provided a point loading effect on a line directly above the specimen slot. Careful attention was given to machining of the loading fixture to insure that good alignment could be achieved during tests.

An MTS Model 632.20B extensometer was used as the displacement gage for accurately measuring the relative displacement of the two gage positions spanning the slot. A pair of accurately machined knife edges were bonded to the specimen with 3M strain gage epoxy and the displacement gage was clipped to these edges to monitor crack opening displacement. Since gage lengths were maintained below one half of the specimen width, displacements were essentially independent of gage length. The displacement gage was calibrated by MTS Corporation in March, 1979, and a range card was also provided by MTS to provide compatibility between the gage and the model 440.21 Transducer Signal Conditioner. The gage provides a linear voltage output over a 0.254 cm range of displacement.

In order to insure the state of stress at the crack front approached the maximum values represented by triaxial plane strain conditions, a fatigue precrack was induced in the specimen through cyclic loading. A sine wave compressive load was generated by the function generator under load control, utilizing the same fixtures used in the fracture toughness test. The ASTM Standard requires that the slot plus precrack measure between 0.45 and 0.55 W (W is the specimen width, Fig. 1.A). Initial attempts were made to monitor the development of the precrack using a photoelastic device but this proved unsuccessful. It was determined that the precrack

advance could be monitored with acceptable results by fatigue cracking one specimen to failure while observing the COD gage output. Subsequent examination of the failed surface provided data which, when combined with the output record of the COD gage, could be used to monitor the precrack advance on other specimens of the same material.

One of the most difficult standard limits to achieve was that the maximum fatigue stress intensity,  $K_f(\text{max})$ , during the final stage of fatigue precracking, for at least the terminal 2.5% of the overall crack plus slot length, must not exceed 60% of the apparent fracture toughness of the material. Since the apparent fracture toughness was not known until after the fatigue loading was completed and subsequent fracture toughness testing accomplished, a number of tests conducted proved to be invalid because this criterion was exceeded. It was necessary to test several specimens of each material by loading to failure, after inducing a precrack, to determine the failure load range which was then used to determine the maximum loading for fatigue precracking of subsequent specimens. It was usually necessary to use a fairly large maximum load during initial fatigue precracking to get the crack started and then reduce this maximum load during the terminal stages of precracking to comply with the standard. The stress-intensity range was kept near the 90% of  $K_f(\text{max.})$  recommended by the standard.

The standard requires that, for test results to be valid, the specimen thickness,  $B$ , and crack length,  $a$ , exceed  $2.5(K_{IC}/\sigma_{YS})^2$ . For these tests, specimen thickness was dictated

by the requirements of the Army Ballistics Research Laboratory at Aberdeen, Maryland, which was funding the material acquisition. As a result, it was not certain that the above criteria for B would be met and, in any case, the minimum value of B could not be ascertained until  $K_Q$  values were obtained from test results and used to determine B.  $K_Q$  is the measured value of stress intensity factor at which crack propagation occurs. If all the other standard requirements are met, and B and a values then exceed the above ratio using  $K_Q$  for  $K_{IC}$ , then  $K_Q$  is considered to be equal to  $K_{IC}$ .

The crack length was controlled by the fatigue precracking as described above. The first specimen design used had a square notch cut, but this proved unreliable for developing precracks. The second design utilized a  $90^\circ$  chevron notch in a slot as shown in Fig. 1.A. The standard recommends a notch root radius of 0.025 cm to facilitate fatigue precracking at a low level of stress intensity. The facilities were not available to provide this radius and so a hardened razor blade was used to cut the tip of the chevron notch with excellent results. Good control of fatigue precrack start and propagation was maintained with this design. Once the fatigue precrack was developed, the fatigue toughness test was conducted by loading the specimen to failure using an inverted ramp signal from the function generator under load control. Loading rates were maintained to keep the stress intensity between 0.55 and 2.75  $\text{MPa}\cdot\text{m}^{1/2}/\text{sec}$  as required by the standard. A Hewlett-Packard plotter was used to provide a graphic record of load-sensing transducer output versus the output of the displacement gage.

### 3. Microscopy Procedures

Samples were sectioned from specimens of each of the alloys tested. The sectioned surface of each sample was sanded flat and polished using alumina micropolish. Each sample was ultrasonically cleaned and the polished surface was immersed in a saturated picral etchant solution. Immersion times varied from 20 seconds to one minute, with best results obtained in the 20-30 second range.

Each sample was examined at 400X on a Bausch and Lomb Balplan microscope and photographs taken of the etched surface. The 53150, 52100 and 10150 UHC steels were examined using a Cambridge Scientific Instruments Limited S4-10 Stereoscan Scanning Electron Microscope (SEM) and photographs were taken of the etched surface of each of these alloys at 6000X and 11000X. Photographs were also taken of the fracture surface of the 52150 UHC steel at 500X, 1500X and 2500X using the SEM. Samples of the 10150 UHC steel taken before and after a one-hour anneal at 650°C were examined and photographed using a Phillips EM 201 Transmission Electron Microscope (TEM) at 20000X to investigate and record dislocation densities, grain sizes and carbide particle distribution. This work was accomplished by Visiting Professor T. Yamashita of the Japan National Defense Academy, Yokosuka, Japan.

### III. RESULTS/DISCUSSION

#### A. MICROSTRUCTURAL ANALYSIS

All alloys tested were processed using the Sherby Process in order to achieve a refined microstructure of spheroidized carbides in a ferrite matrix. The ferrite grain size is a function of alloying content as well as degree of warm rolling; chromium, in particular, tends to stabilize the spheroidal carbide particle size and thus help to restrict the degree of ferrite grain growth.

##### 1. Light Microscope

Figures 4-8 illustrate the microstructure of 52150, 53150, 43150, 10150, and 52100 UHC steels, respectively. The 52150, 53150 and 52100 UHC steels were etched using a saturated picral etchant solution while 43150 and 10150 UHC steels were etched with a 2% nital etchant solution. Examination of micrographs reveals a very similar microstructure in all the steels with the exception of the 10150 UHC steel. The others all have some relatively coarse carbides, aligned in the rolling direction, mixed with very fine spheroidal carbides in a ferrite matrix. The 52100 UHC steel (Fig. 8) appears to have a lesser percentage of the coarse carbides than the other three steels but some very large carbides in long strings are evident in the material.

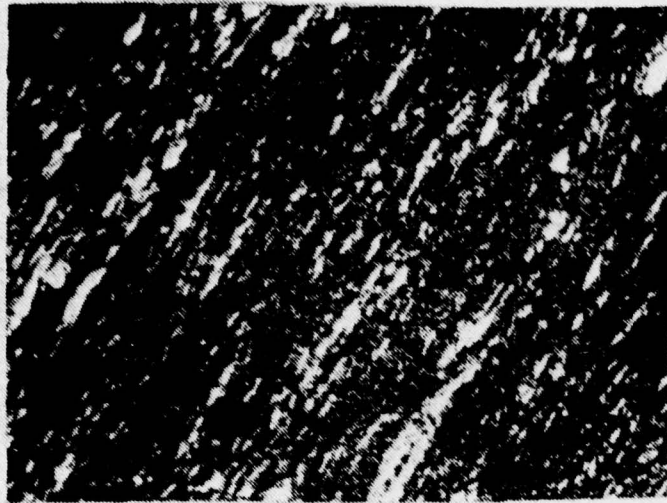


Fig. 4. Micrograph of 52150 UHC steel etched in a saturated picral solution for one minute. Microstructure consists of coarse carbides mixed with fine carbides in a ferrite matrix. 400X

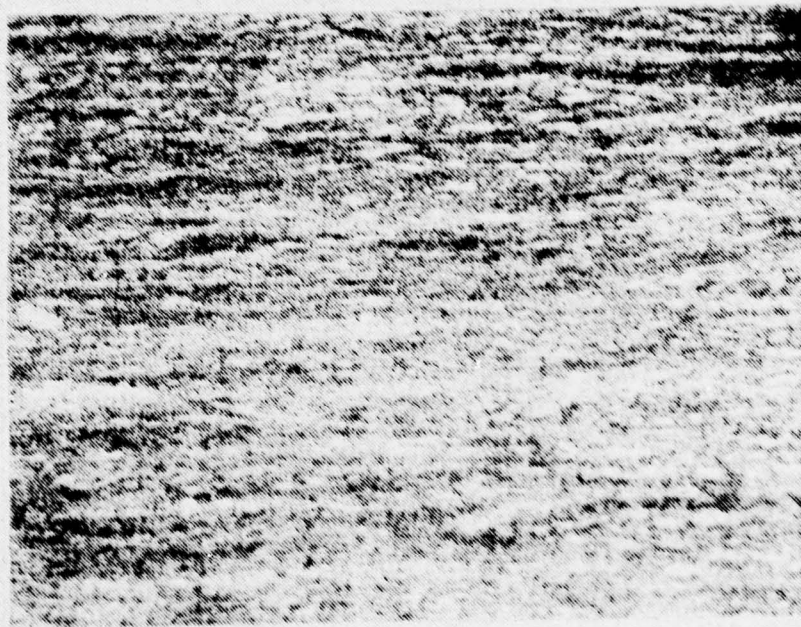


Fig. 5. Micrographs of 53150 UHC steel etched in a saturated picral solution for 30 seconds. Microstructure consists of coarse carbides mixed with fine carbides in a ferrite matrix. 400X

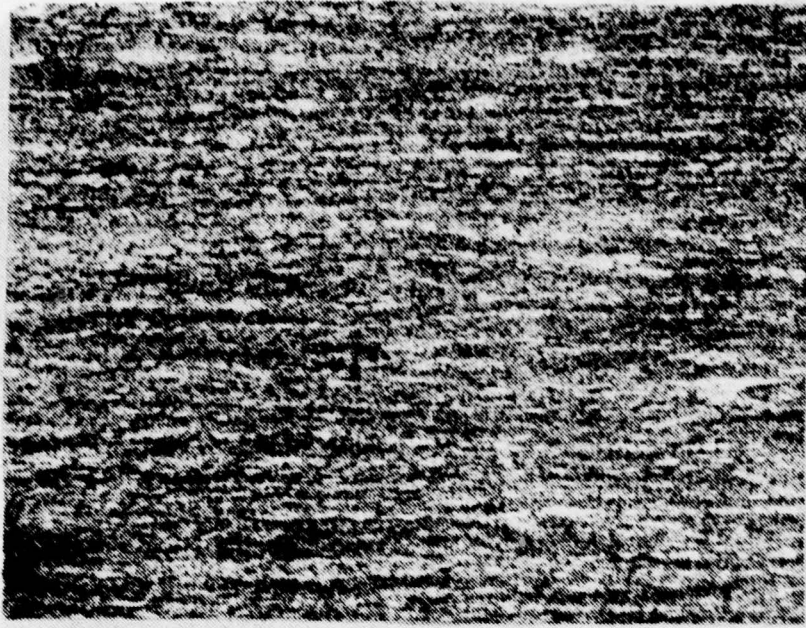


Fig. 6. Micrograph of a 43150 UHC steel etched in a 2% nital solution for 20 seconds. Microstructure consists of coarse carbides mixed with fine carbides in a ferrite matrix. 400X

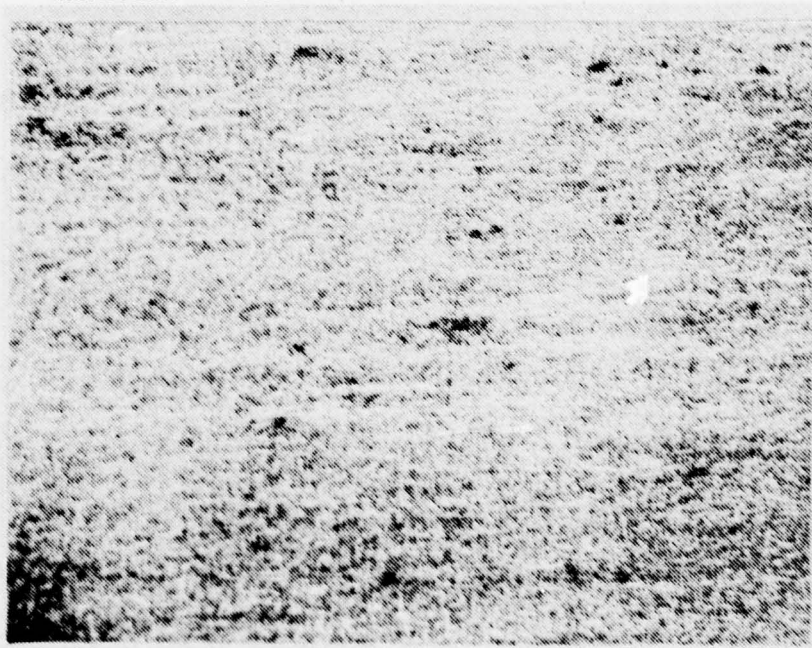


Fig. 7. Micrograph of a 10150 UHC steel etched in a 2% nital solution for 20 seconds. Microstructure consists of spheroidal carbides of fairly uniform size in a ferrite matrix. 400X



Fig. 8. Micrographs of 52100 UHC steel etched in a saturated picral solution for 25 seconds. Microstructure consists of coarse carbides mixed with fine carbides in a ferrite matrix. 400X

## 2. SEM

The 10150 UHC steel in Fig. 7 shows no evidence of coarse carbides but the spheroidal carbides in the microstructure are much larger on the average than the fine carbides in the other materials. This is particularly evident in Figs. 9 and 10, which show 10150 and 52100 UHC steels at 11000X, and Fig. 11, which shows 52150 UHC steel magnified at 13000X; all of these micrographs were made in the SEM. While the 52150 UHC steel in Fig. 11 has most of its spheroidal carbides much smaller than those in the 10150 UHC steel in Fig. 9, it also has several carbides which are much larger than those in the 10150 UHC steel. The 52100 UHC steel in Fig. 10 has the finest spheroidal carbide microstructure of all the materials examined. While no coarse carbides are evident in Fig. 10, they did exist in other areas of the etched surface. Figure 12 is another region of the 52150 UHC steel at 2550X, showing how the coarse carbides are aligned in stringers; this type of structure was observed in all the steels containing coarse carbides.

An examination in the SEM was made of the microstructure at the fracture surface of a 52150 UHC steel specimen broken in a Charpy Impact Test. Impact testing was accomplished over a range of temperatures. Figure 13 shows the microstructure of the fracture surface of a sample fractured at room temperature. The surface shows no evidence of ductile fracture and appears to have failed by cleavage. Figure 14 shows the same material fractured at 100°C and again the fracture mechanism appears to be some form of cleavage. Figure 15 shows the same result in



Fig. 9. Micrographs of a 10150 UHC steel etched in a 2% nital solution for 20 seconds. Many spheroidal carbides in the one micron diameter region are evident. 11000X

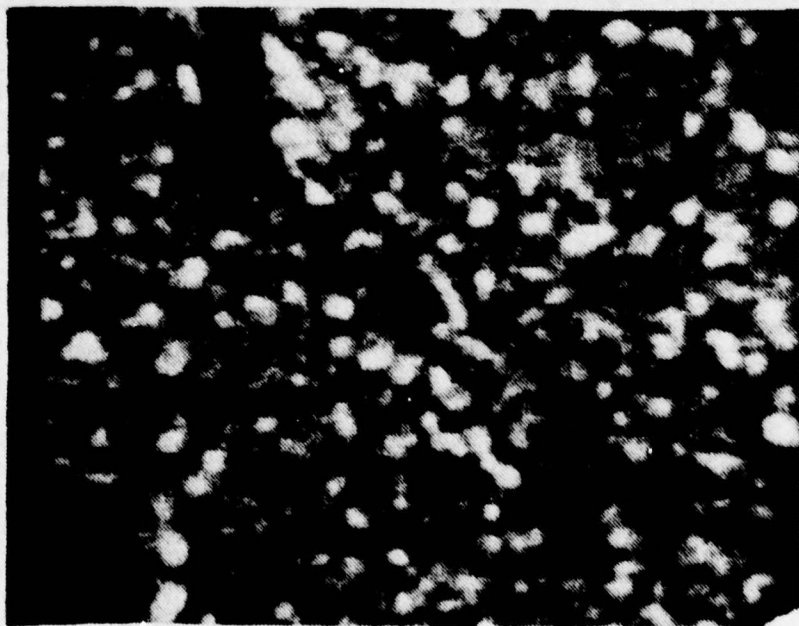


Fig. 10. Micrographs of a 52100 UHC steel etched with a saturated picral solution for 25 seconds. Spheroidal carbides are very fine with none visible over one half micron diameter. 11000X

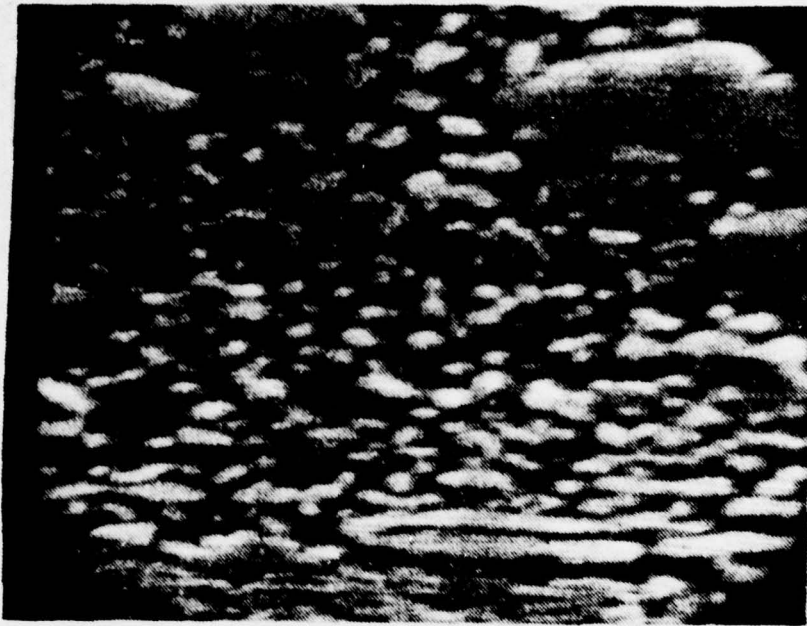


Fig. 11. Micrograph of 52150 UHC steel etched in a saturated picral solution for 25 seconds. Most spheroidal carbides are less than one half micron diameter with some large carbides over four microns across. 13000X



Fig. 12. Micrograph of 52150 UHC steel etched in a saturated picral solution for 25 seconds. This region has very coarse carbides aligned in the rolling direction. 2550X

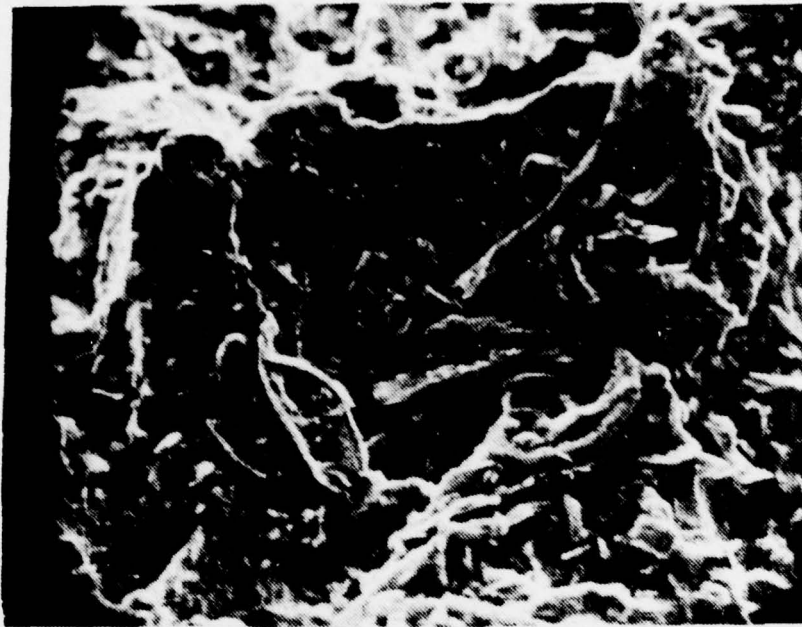


Fig. 13. Micrograph of fracture surface of 52150 UHC steel fractured at room temperature in a Charpy Impact Test. Surface condition indicates a cleavage fracture mode. 1500X

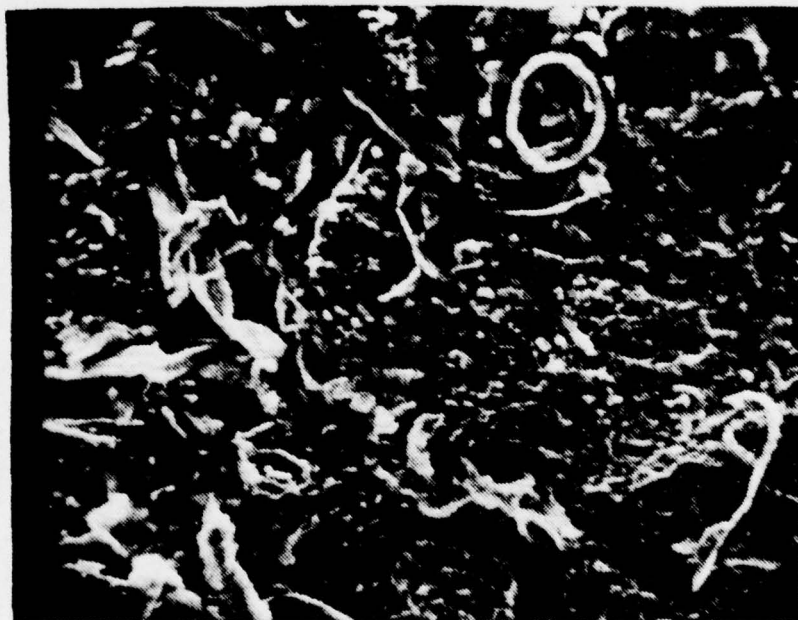


Fig. 14. Micrograph of fracture surface of 52150 UHC steel fractured at 100°C in a Charpy Impact Test. Surface condition indicates a cleavage fracture mode. 1280X

a specimen fractured at 220°C, which is near the maximum temperature usable for this test. Elevating temperature did not bring about the anticipated transition to a more ductile failure mechanism for samples failing under a high strain-rate loading. A surprising observation from these fracture surfaces (and also Ref. 8) was that coarse carbides did not appear to provide the route chosen by the crack for propagation, although such carbides generally do provide the route in a high carbon steel because of their brittle nature.

### 3. Macro Examination

Figure 16 is an example of the fatigue crack appearance on a fracture toughness specimen. The crack has propagated from the chevron notch into the material. Final failure occurred by unstable crack propagation from the fatigue pre-crack during a slow, continuous load increase to failure. The fracture surface is very flat with little evidence of shear lips. This fatigue crack front would invalidate the fracture toughness test as it has too much of a clamshell shape rather than the straight crack front required by Ref. 4.

### 4. TEM

Figure 17 is a TEM micrograph of 10150 UHC steel at 10000X. It is evident that there is a finer spheroidal carbide microstructure than was observed in Fig. 7. The carbides visible are less than one micron in diameter and this is consistent with the results of the Sherby Process for the other steels examined. Figure 18 is a TEM micrograph of the same steel at 20000X. The dark lines visible represent piled up dislocations and the high density of those

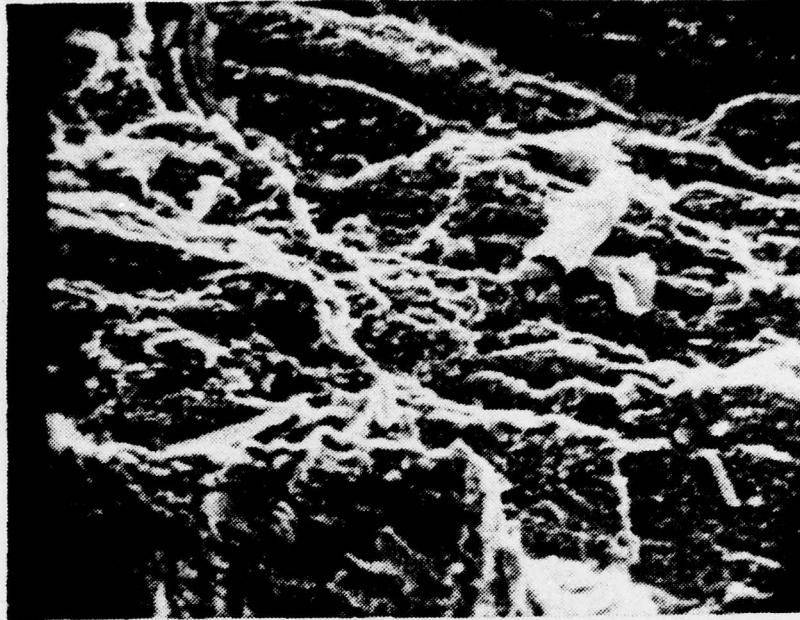


Fig. 15. Micrograph of 52150 UHC steel fractured at 220°C in a Charpy Impact Test. Surface conditions indicate a cleavage fracture mode. 1200X



Fig. 16. Micrograph of 52150 UHC steel fractured in a fracture toughness test. A clamshell shaped fatigue crack front has propagated from the chevron notch. Fracture surface is very flat. 20X



Fig. 17. Micrograph of 10150 UHC steel as rolled taken at a  $6^\circ$  tilt angle with a TEM. Spheroidal carbides are visible as dark balls in the lighter ferrite matrix. 10000X



Fig. 18. Micrograph of 10150 UHC steel taken with TEM at 20000X. Subgrain boundaries are clearly visible. Black lines represent a high density of dislocations in the microstructure.

lines in this picture is indicative of the large amount of working the material has undergone. This dislocation density may help explain the poor toughness exhibited by this material considering its low relative strength, as it is already highly work hardened. Figure 19 is a micrograph of a selected-area diffraction pattern for the 10150 UHC steel. While this pattern is not indexed with the area in Fig. 18, it is taken from that region and the aperture of five microns indicates that grain size is in excess of this value, since there is no superposition on the diffraction pattern. This indicates that the ferrite grains are larger than was anticipated after being worked by the Sherby Process and that the boundaries visible in Fig. 18 represent a subgrain structure. The carbides did not act as effectively as hoped as pinning agents to produce a fine ferrite grain size.

Figure 20 is a TEM micrograph of the 10150 UHC steel after a one-hour anneal at 650°C, followed by an air cool to room temperature. The dislocation density is reduced in this structure over that observed in the as-rolled condition. Webs of dislocations are still visible, however, at some of the subgrain boundaries of the structure.

## B. MECHANICAL TESTING RESULTS

The tensile, hardness and impact properties of the UHC steel alloys are a result of both alloying content and amount of rolling deformation accomplished. Since the same processing was accomplished on all the steel alloys, the difference in

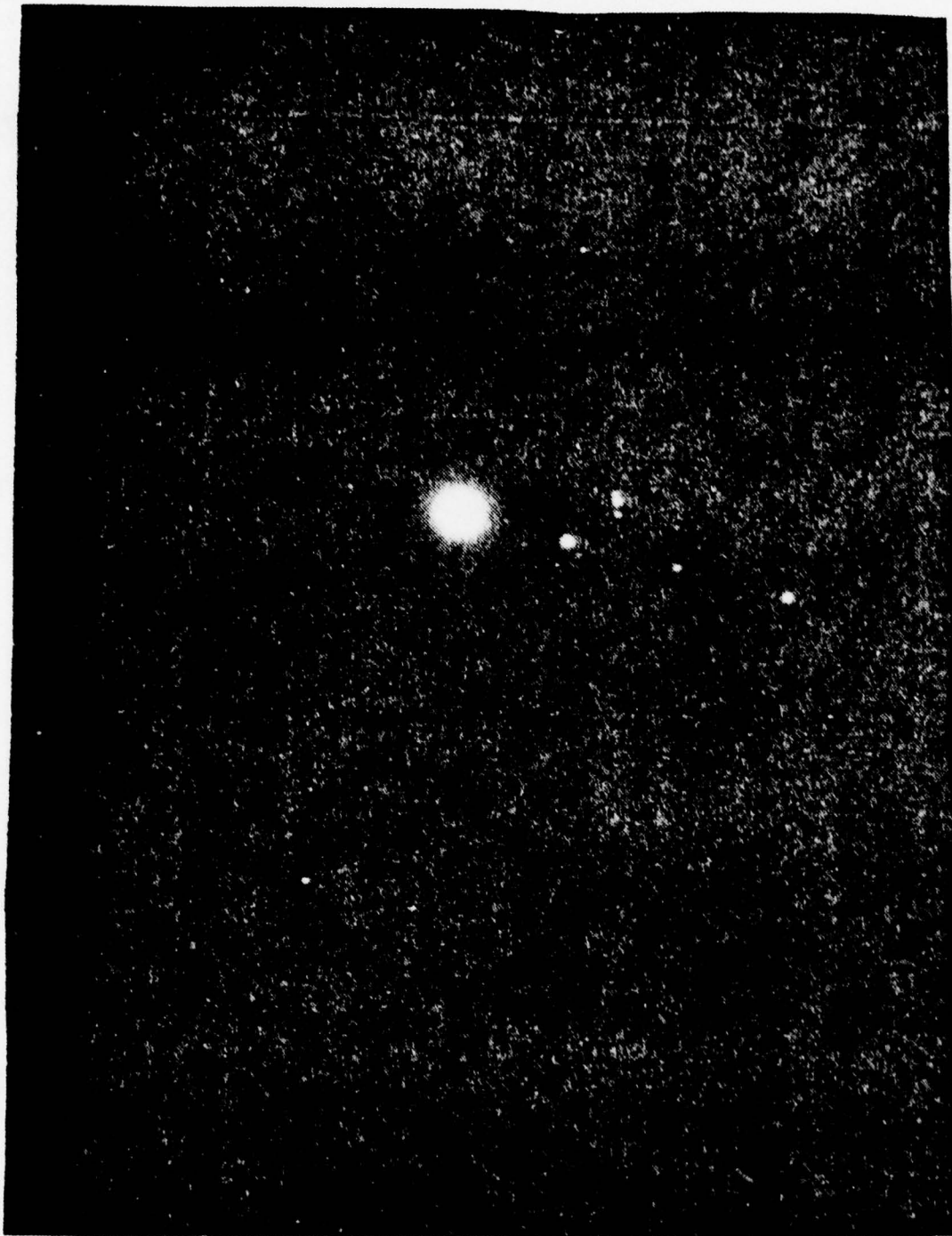


Fig. 19. Micrograph of 1015 UHC steel taken with TEM. This one second exposure clearly shows the defraction pattern of the crystal structure.



Fig. 20. Micrograph of 10150 UHC steel annealed at 650°C taken with TEM. Dislocation density is reduced from that noted in Fig. 18. 20000X

these properties for the materials tested is more a function of alloying. In the case of two of the steels, 53150 and 10150, a one-hour anneal at 650°C was utilized and its effect also examined.

1. 52150-1 UHC Steel as Rolled

This material had a yield strength of 951.4 MPa, an ultimate tensile strength of 1063.9 MPa and an elongation to fracture of 10.3%. The hardness in the as-rolled condition was  $R_c$  33.0. The material had very low energy absorption, 2.4 joules, on the Charpy V-Notch Impact Test and broke in a brittle mode (Fig. 13).

2. 52150-2 UHC Steel as Rolled

This second heat of the 52150 material had slightly higher yield strength at 972.1 MPa and an ultimate tensile strength of 1078.9 MPa, but reduced ductility (7.6% elongation to fracture). The hardness was  $R_c$  35.0 but the impact absorption energy was only 0.7 joules and the surface appearance indicated a brittle fracture mode.

3. 53150 UHC Steel as Rolled

The tensile strength of this higher chromium alloy was up, with a yield strength of 1041.0 MPa and an ultimate tensile strength of 1184.4 MPa. Ductility was again low with 7.1% elongation to fracture. Hardness was  $R_c$  36.0. This material also had a very low impact energy absorption, 1.4 joules. Tensile properties were not determined on the 53150 UHC steel annealed at 650°C for one hour, but hardness remained unchanged.

4. 43150 UHC Steel as Rolled

This material exhibited the highest yield strength of those steels tested, with a yield strength of 1067.2 MPa, and had an ultimate tensile strength of 1104.7 MPa. Ductility was a disappointing 3.0% elongation to fracture. This material also exhibited the highest as-rolled hardness at  $R_c$  39.5. Impact absorption energy was slightly improved at 3.1 joules but was still well below expected performance on the Charpy Impact Test.

5. 10150 UHC Steel as Rolled

Tensile data was not obtained on this material due to the unavailability of tensile samples but hardness was determined for the material as rolled and after a one-hour anneal at 650°C with a subsequent air cool to room temperature. Hardness dropped from  $R_c$  21.5 for the as-rolled material to  $R_c$  19.5 after the anneal.

6. 52100 UHC Steel as Rolled

This material had the lowest strength, with the exception of the 10150 UHC steel which was not checked. Yield strength was 861.0 MPa and ultimate tensile strength was 956.9 MPa. The material had good ductility, with 16.5% elongation to fracture. Hardness was good for this lower strength steel at  $R_c$  36.0. This steel was by far the best performer on the Charpy Impact Test with an impact absorption energy of 19.0 joules.

Table II provides a summary of the mechanical testing results. The results were unusual in that ductility was lower

TABLE II

## PROPERTIES OF TESTED ULTRA-HIGH CARBON STEEL ALLOYS

Alloy	Tensile Properties		Percent Elongation (1)	Fracture Properties			Hardness HRC
	Elongation KSI (MPa)	Ultimate Tensile Strength KSI (MPa)		Charpy V-Notch Impact Test Ft-lb (Joules)	Apparent Fracture Toughness KSI-in <sup>1/2</sup> (MPa·m <sup>1/2</sup> )	Specimen Strength Ratio	
52150-1 as rolled	138.0 (951.4)	154.2 (1063.9)	10.3	1.8 (2.44)	46/(51)	1.11	33.0
52150-2 as rolled	141.0 (972.1)	156.5 (1078.9)	7.6	0.5 (0.68)	49/(54)	1.18	35.0
53150 as rolled 650°C anneal	151.0 (1041.0)	171.8 (1184.4)	7.1	1.0 (1.36)	46/(51)	1.09	36.0
43150 as rolled	158.4 (1067.2)	160.2 (1104.7)	3.0	2.25 (3.05)	41/(46)	0.87	39.5
10150 as rolled 650°C anneal	(2)	112.0 (772.1)			54/(59)		21.5
52100 as rolled	127.8 (861.0)	138.8 (956.9)	16.5	14.0 (19.04)	78/(86)	2.51	36.0

NOTE: (1) Elongation by .2% offset method

(2) Tensile test not conducted on 10150. UTS approximate from hardness.

than expected for the 52150-2, 53150 and 43150 UHC steels and the impact absorption energy was very poor for all the steels tested except 52100 UHC steel. Since the impact energy absorption is the property most closely associated with toughness among those properties examined, this result was not promising as a predictive measure of the steels' fracture toughness.

### C. FRACTURE TOUGHNESS TESTING RESULTS

One of the major goals of this research effort was the measurement of the fracture toughness, i.e. resistance to unstable crack propagation, of the materials examined. The procedures for conducting this test have already been described and the following is an outline of how the test results were calculated and interpreted. This is followed by a description of the results for each material examined.

Once a fracture toughness test has been conducted, the results must be examined against a set of criteria set forth in Ref. 4 to determine if a valid  $K_{IC}$  has been determined. At least three valid tests should be conducted for each material and the results averaged. Some of the criteria were described in the fracture toughness testing procedure section and the remainder are outlined below. A tangent line was drawn to the initial part of the graphic record of each test conducted. A secant line with a slope equal to 95% of the tangent line was then constructed and the highest load up to the point of intersection of this line with the

load displacement curve was defined as  $P_Q$ . The ratio of  $P_{\max}/P_Q$  was then calculated and if this exceeded 1.10 the test was invalid.

The fracture surface of the specimen was examined and the fatigue precrack length was measured. In order for the test to be valid, the precrack length at the center of the crack front and at the midpoint between the center and each side of the crack front must have been within 5% of the average of these three values. No part of the crack front could be closer to the machined notch root than 5% of the average crack length, or 0.13 cm, and the length of either surface trace of the crack had to be more than 90% of the average crack length. The crack plane had to be parallel to both the specimen width and thickness directions within  $\pm 10$  degrees.

When the above criteria were all met, a conditional result was calculated as follows

$$K_Q = \frac{(P_Q \cdot S)}{(B \cdot W^{3/2})} \cdot f\left(\frac{a}{W}\right) \quad (1)$$

where

$$f\left(\frac{a}{W}\right) = \frac{3\left(\frac{a}{W}\right)^{1/2} \left[1.99 - \left(\frac{a}{W}\right) \left(1 - \frac{a}{W}\right) \left(2.5 - \frac{3.93a}{W} + \frac{2.7a^2}{W^2}\right)\right]}{2\left(1 + \frac{2a}{W}\right) \left(1 - \frac{a}{W}\right)^{3/2}} \quad (2)$$

This result was then used to calculate the quantity

$$B' = 2.5 \left(\frac{K_Q}{\sigma_{YS}}\right)^2 \quad (3)$$

If  $B'$  was less than both the crack length and the specimen thickness, then the  $K_Q$  value was considered equal to  $K_{IC}$  [Ref. 4].

When the fracture toughness test failed to meet one or more of the criteria in Ref. 4 the specimen strength ratio, a nondimensional term when consistent units are used, was calculated as follows

$$R_{sb} = \frac{6 P_{\max}}{B(W-a)^2 \sigma_{YS}} \quad (4)$$

These ratios were also calculated for tests resulting in valid  $K_{IC}$  values. The specimen strength ratio is dependent on form and size of the specimen as well as material. This ratio can be a useful measure of the comparative fracture toughness of two or more materials "when the results are compared from specimens of the same size and form and when this size is sufficient that the limit load of the specimen is a consequence of pronounced crack extension prior to plastic instability" [Ref. 4]. Because of the strengths and thicknesses of the steels tested, it was not actually desirable to find that a valid  $K_{IC}$  could be determined. The small thicknesses available meant that this value would be small and the material, therefore, not very tough if, in fact, a valid  $K_{IC}$  were measured. Table II contains a summary of the fracture toughness test results.

1. 53150 UHC Steel as Rolled

Table III and Figs. 21 and 22 provide a record of the test results for this material. A valid  $K_{IC}$  value of  $51 \text{ MPa}\cdot\text{m}^{1/2}$  was determined for this material. Four valid tests were conducted with a 6.7% variation in test results, good reproducibility for this test. Fracture surfaces were

Table III

Results of Fracture Toughness Tests  
for 53150 UHC Steel Alloy as Rolled

	Test I	Test II	Test III	Test IV
Thickness B (cm)	0.693	0.693	0.693	0.693
Depth W (cm)	1.280	1.285	1.283	1.283
$K_f$ max (MPa-m <sup>1/2</sup> )	28.03	28.75	28.65	29.39
Stress Intensity Range for Terminal Crack Extension (MPa-m <sup>1/2</sup> )	25.23	23.00	19.10	23.51
Crack Length (cm) left	0.597	0.617	0.572	0.627
center	0.615	0.635	0.584	0.648
right	0.620	0.706	0.597	0.630
Crack Length (cm) left at Surface	0.554 0.564	0.572 0.589	0.536 0.533	0.564 0.574
right				
Number of Cycles for Terminal Fatigue Crack	58990	111990	14450	6400
Test Temperature (°C)	21	21	21	21
Relative Humidity				
Loading Rate in Terms of $K_I$ (MPa-m <sup>1/2</sup> /s)	0.58	1.15	0.96	1.18
Crack Plane Orientation	T-L	T-L	T-L	T-L
Fracture Appearance (fraction oblique)	.11	.05	.09	.10
Yield Strength (offset = .2%) (MPa)	1041.0	1041.0	1041.0	1041.0
$K_{IC}$ (MPa-m <sup>1/2</sup> )	49	50	52	52
$R_{sb}$	1.02	0.97	1.24	1.09
$\frac{P_{max}}{P_Q}$	1.10	1.02	1.09	1.08



Fig. 21. Graphs of 53150 UHC steel tests one and two, respectively. Both graphs are Type I records and both records are for valid  $K_{IC}$  tests.

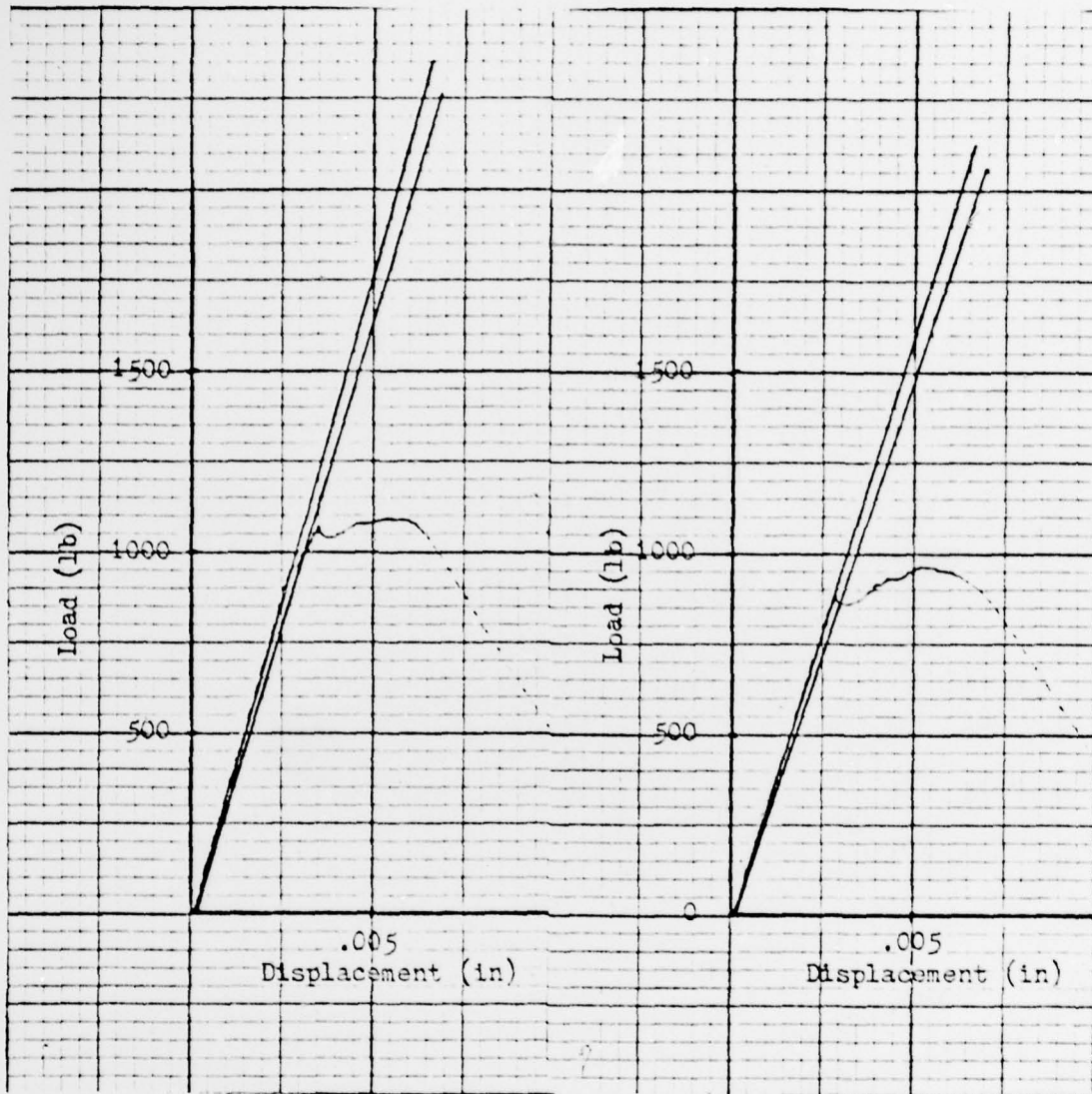


Fig. 22. Graphs of 53150 UHC steel tests three and four, respectively. Graph three is a Type I record and graph four is a Type II record. Both records are for valid  $K_{IC}$  tests.

very flat with only a small shear lip evident at the edges of the specimen and the specimen appeared to have failed in a brittle manner. All specimens were cut with a longitudinal long-transverse orientation. Three load displacement records were Type I records in that the load at the secant line intersection with the graph exceeded all the loads that preceded it. The fourth test was a Type II record with  $P_Q$  preceding the secant line intersection. The reason for the large variation in fatigue precracking cycles from the first test to the other three was the difficulty in determining the maximum fatigue load permissible for final crack propagation. Once this was determined in the first test, the load was adjusted accordingly for the remaining tests. The average specimen strength ratio was 1.11.

## 2. 43150 UHC Steel as Rolled

Table IV and Figs. 23 and 24 provide a record of the test results for this material. A valid  $K_{IC}$  value of  $46 \text{ MPa}\cdot\text{m}^{1/2}$  was obtained for this material. Three valid tests were conducted with a 7.3% variation in test results, again good reproducibility for this test. In addition, a fourth test (Test II) was completed with a  $K_Q$  value of  $44 \text{ MPa}\cdot\text{m}^{1/2}$ , but this was an invalid  $K_{IC}$  result since the maximum fatigue stress intensity during terminal fatigue precracking was 82% of the subsequently determined  $K_Q$  vice the maximum permissible 60%. This was the result of unstable crack propagation to failure at a lower than anticipated load due to fatigue precrack which had extended deep into the material. The load displacement records were all Type I records. Fracture surfaces were relatively flat with

Table IV

Results of Fracture Toughness Tests  
for 43150 UHC Steel Alloy as Rolled

	Test I	Test II	Test III	Test IV
Thickness B (cm)	0.721	0.721	0.722	0.721
Depth W (cm)	1.275	1.275	1.275	1.273
$K_f$ max (MPa-m <sup>1/2</sup> )	25.45	36.03	27.59	26.26
Stress Intensity Range for Terminal Crack Extension (MPa-m <sup>1/2</sup> )	20.36	26.20	22.07	21.63
Crack Length (cm) left	0.564	0.693	0.610	0.655
center	0.589	0.686	0.627	0.663
right	0.594	0.678	0.630	0.663
Crack Length (cm) left	0.533	0.620	0.579	0.612
at Surface right	0.549	0.638	0.561	0.620
Number of Cycles for Terminal Fatigue Crack	15400	76500	11000	9300
Test Temperature	22	22	22	22
Relative Humidity				
Loading Rate in Terms of $K_I$ (MPa-m <sup>1/2</sup> /s)	1.02	1.31	1.10	1.24
Crack Plane Orientation	T-L	T-L	T-L	T-L
Fracture Appearance (fraction oblique)	.04	.04	.02	.02
Yield Strength (offset = .2%) (MPa)	1067.2	1067.2	1067.2	1067.2
$K_{IC}$ (MPa-m <sup>1/2</sup> )	47	44 (1)	46	44
$R_{sb}$	0.86	0.90	0.87	0.87
$\frac{P_{max}}{P_Q}$	1.01	1.05	1.02	1.04

NOTE: (1) Invalid IAW section 7.4.2 of ASTM E399-78

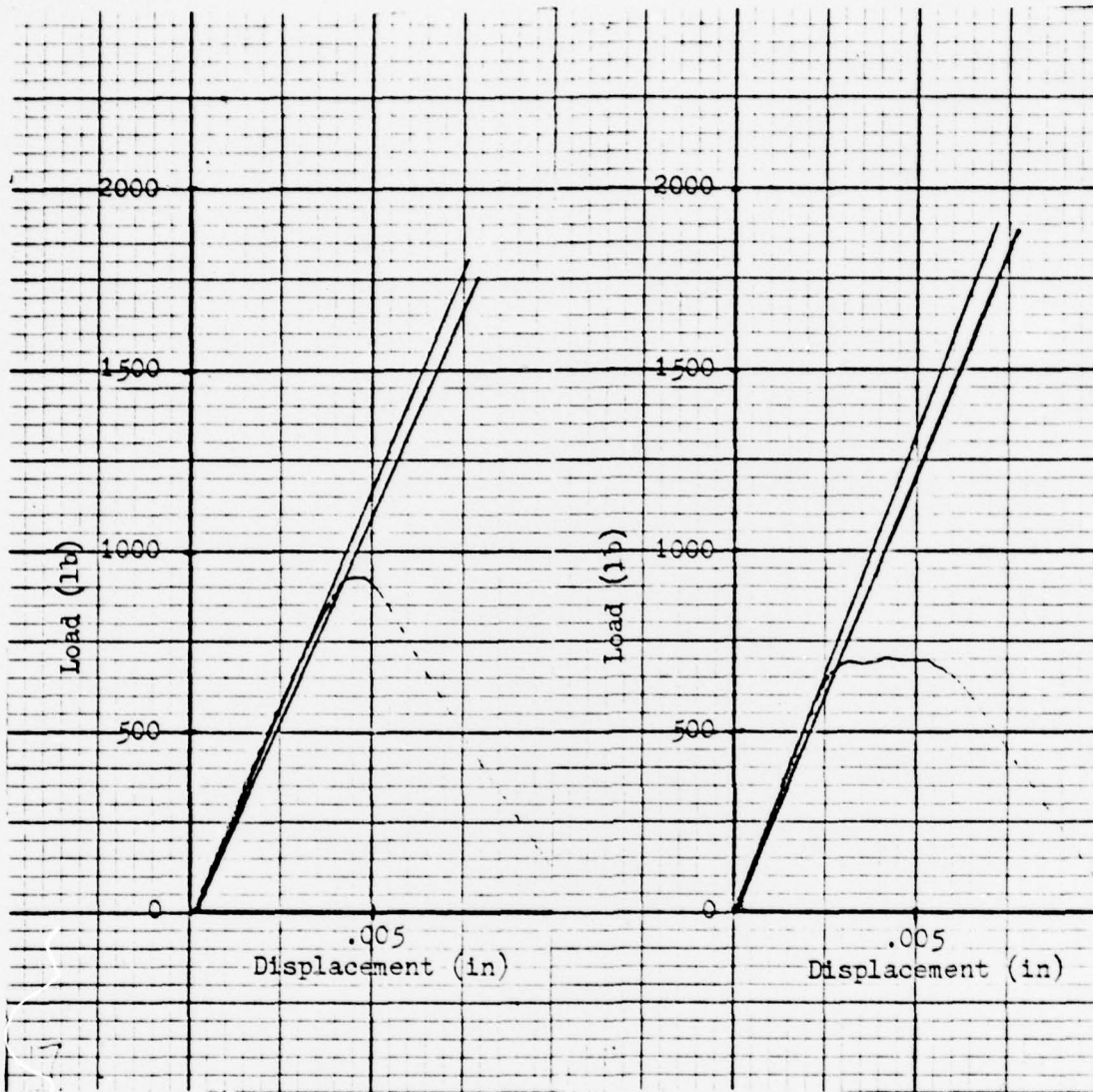


Fig. 23. Graphs of 43150 UHC steel tests one and two, respectively. Both are Type I records. Graph one is a valid  $K_{IC}$  test record while graph two was invalid due to an excessive maximum fatigue stress intensity.

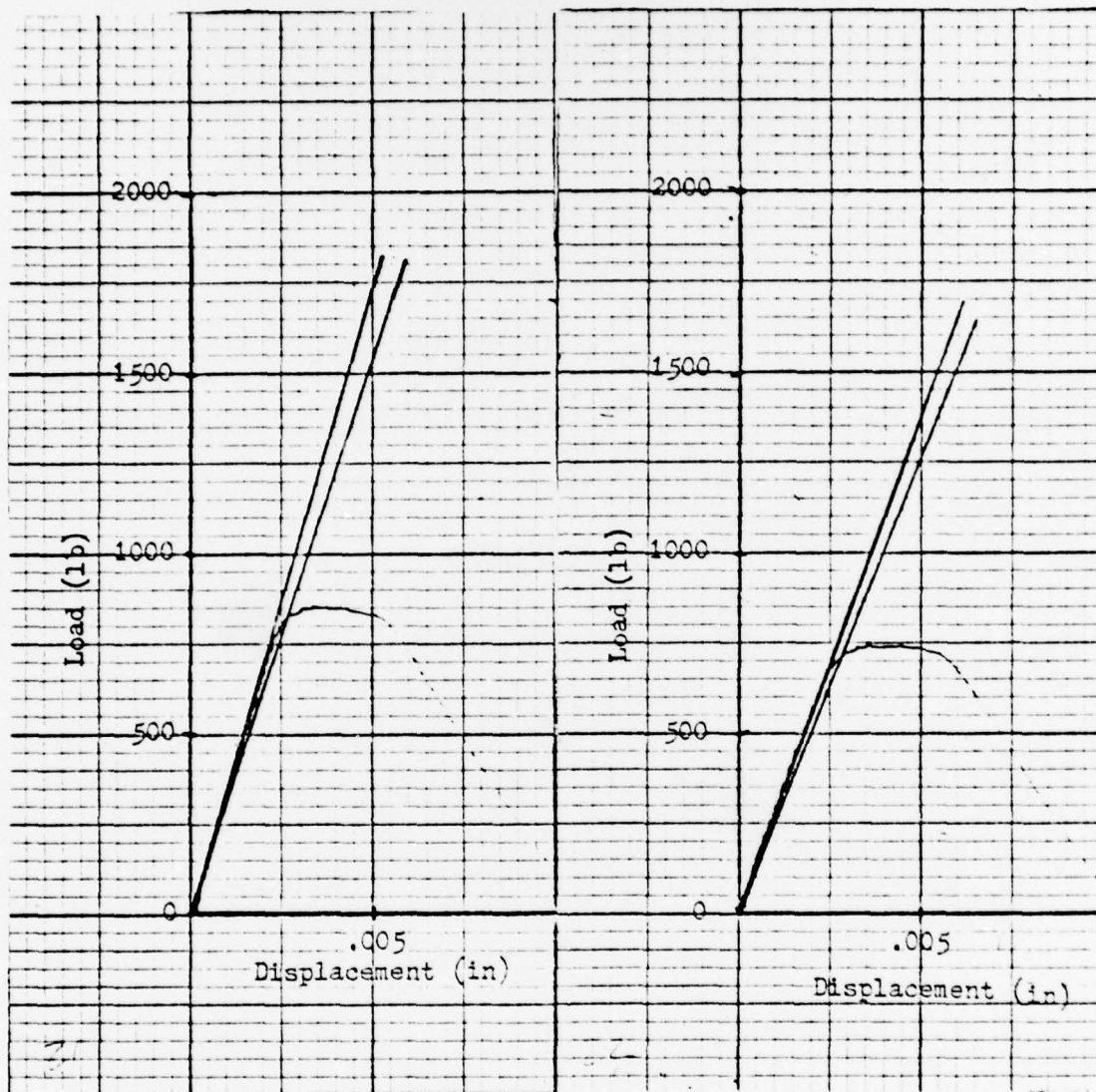


Fig. 24. Graphs of 43150 UHC steel tests three and four, respectively. Both are Type I records and both records are from valid  $K_{IC}$  tests.

almost no shear lips in evidence. The mode of failure appeared to be brittle. The average specimen strength ratio was 0.87. The fracture toughness of this material was 10% below that calculated for the 53150 UHC steel. All specimens were cut with a longitudinal long-transverse orientation.

### 3. 52100 UHC Steel as Rolled

Table V and Figs. 25 through 28 provide a record of the test results for this material. It was not possible to determine a valid  $K_{IC}$  for this material because it proved to be too tough a material to measure this characteristic with the specimen thicknesses available. As is evident in Figs. 25 through 28, the ratio of  $P_{max}/P_Q$  is well in excess of the maximum value permitted by Section 9.1.2 of Ref. 4. The specimen thickness required for a valid test based on the evaluation of the parameter

$$2.5 \left( \frac{K_Q}{\sigma_{YS}} \right)^2$$

was approximately four times the thickness actually available. Fracture surface appearance was very different from the other materials examined, with almost no flat regions and several parallel ridges in the specimen interior running in the fracture direction. Each fatigue precrack region also contained one or more ridges. The surface condition indicated some complex mode of cleavage fracture. The load-displacement records were all Type I, but three of the four records had distinctive crack pop-in regions beyond the secant line intersection. In addition, all graphs had numerous small steps indicating that this steel was able to effectively resist unstable crack propagation by

Table V

Results of Fracture Toughness Tests  
for 52100 UHC Steel Alloy as Rolled

	Test I	Test II	Test III	Test IV
Thickness B (cm)	0.754	0.744	0.739	0.744
Depth W (cm)	1.275	1.260	1.262	1.270
$K_f$ max (MPa-m <sup>1/2</sup> )	33.07	43.51	45.61	49.29
Stress Intensity Range for Terminal Crack Extension (MPa-m <sup>1/2</sup> )	28.35	38.68	40.54	43.81
Crack Length (cm) left	0.561	0.589	0.556	0.612
center	0.579	0.587	0.597	0.645
right	0.564	0.554	0.589	0.607
Crack Length (cm) left	0.528	0.518	0.508	0.516
right	0.536	0.508	0.511	0.513
Number of Cycles for Terminal Fatigue Crack	3300	33300	41700	38900
Test Temperature (°C)	24	24	24	24
Relative Humidity				
Loading Rate in Terms of $K_I$ (MPa-m <sup>1/2</sup> )	0.95	0.97	1.01	1.10
Crack Plane Orientation	T-L	T-L	T-L	T-L
Fracture Appearance (fraction oblique)	.20	.25	.18	.21
Yield Strength (offset = .2%) (MPa)	861.0	861.0	861.0	861.0
$K_{IC}$ (MPa-m <sup>1/2</sup> )	82 (1)	85 (2)	89 (1)	88 (1)
$R_{sb}$	2.40	2.64	2.43	2.55
$\frac{P_{max}}{P_Q}$	1.33	1.48	1.26	1.29

NOTE: (1) Invalid IAW sections 7.1.3 and 9.1.2 of ASTM E399-78  
(2) Invalid IAW sections 7.1.3, 7.2.1 and 9.1.2 of ASTM E399-78

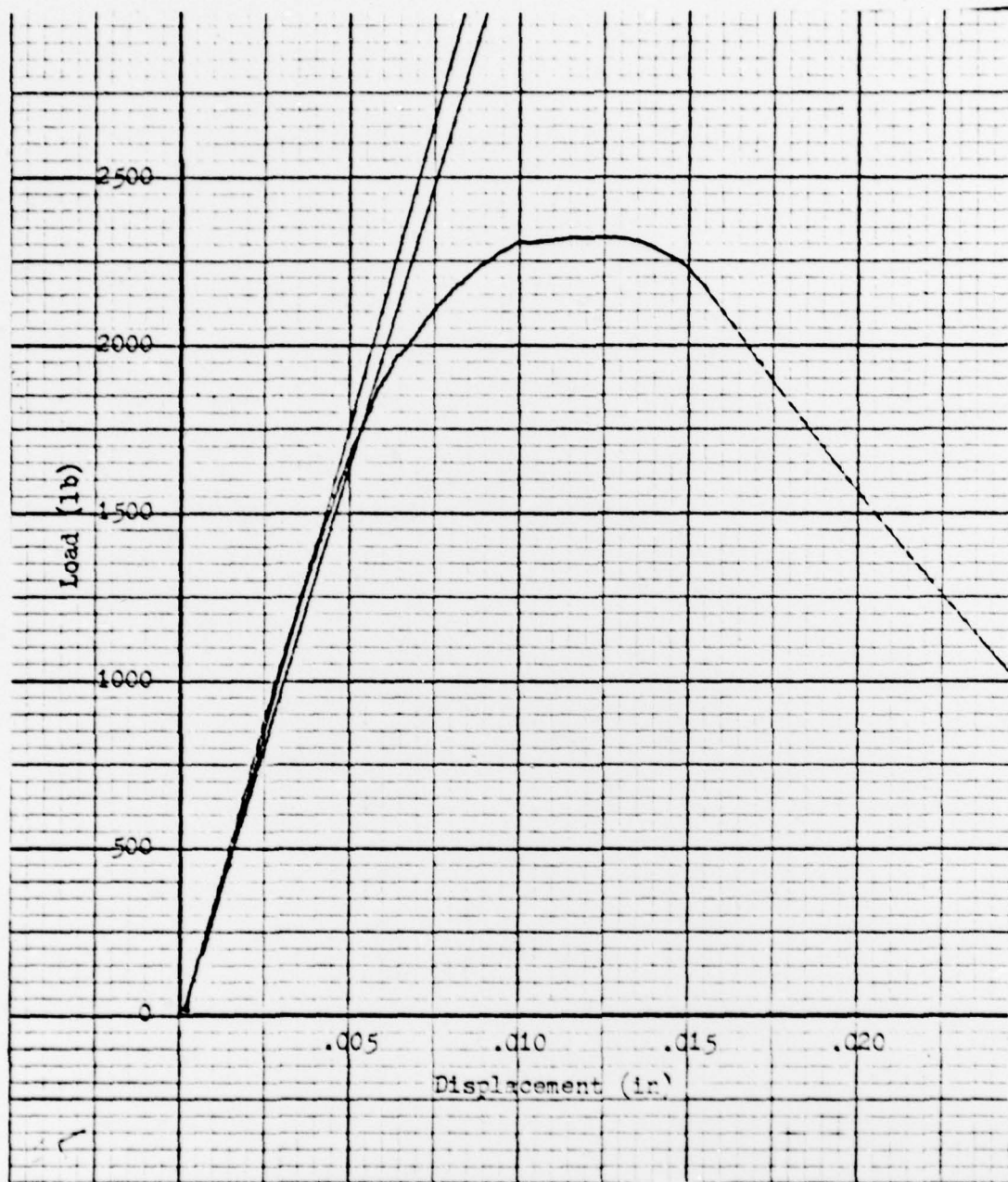


Fig. 25. Graph of 52100 UHC steel test one. This is a Type I record. The results were invalid for  $K_{IC}$ .

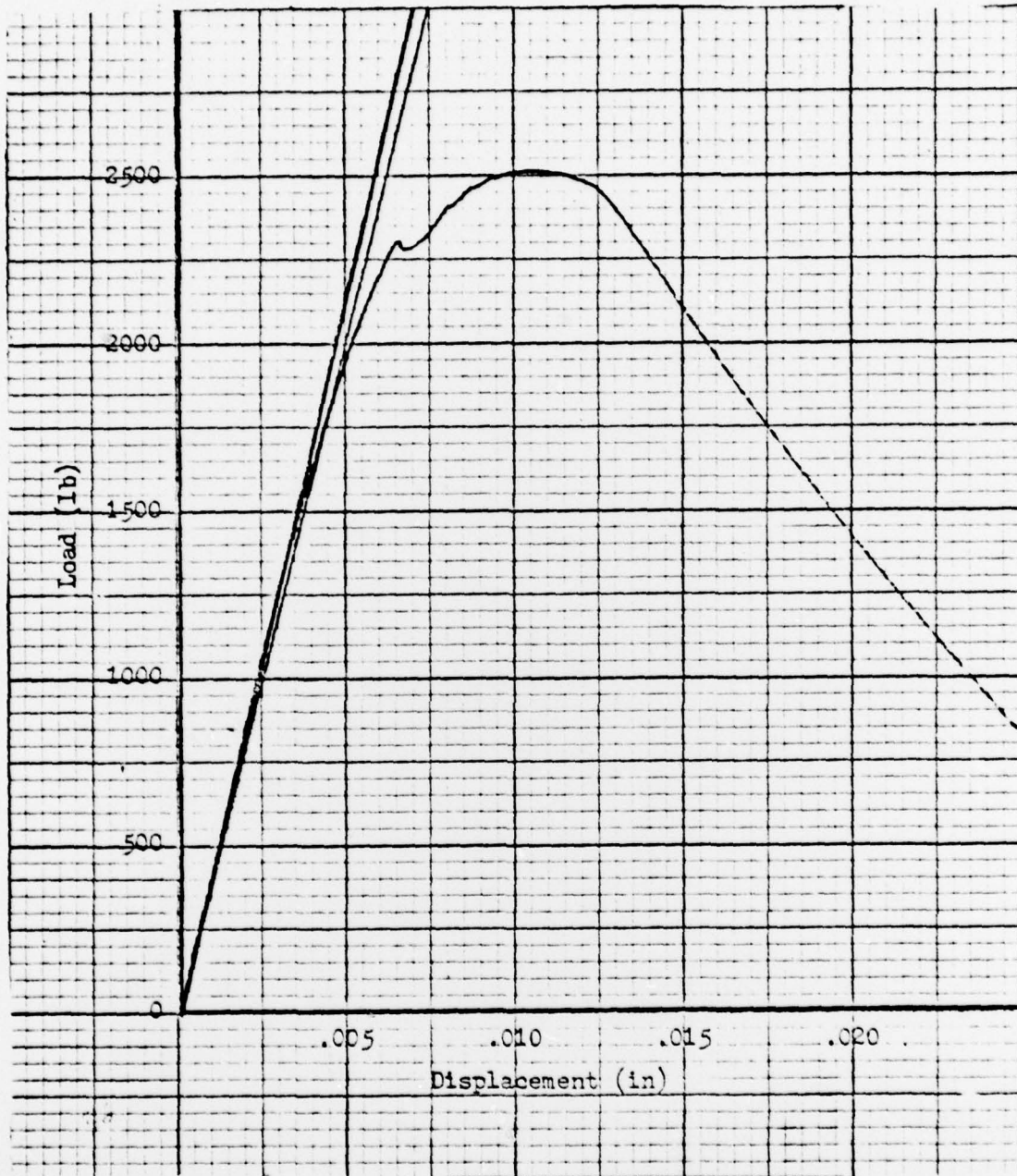


Fig. 26. Graph of 52100 UHC steel test two. This is a Type I record. The results were invalid for  $K_{IC}$ . Note the distinctive pop-in crack step at 2300 lbs.

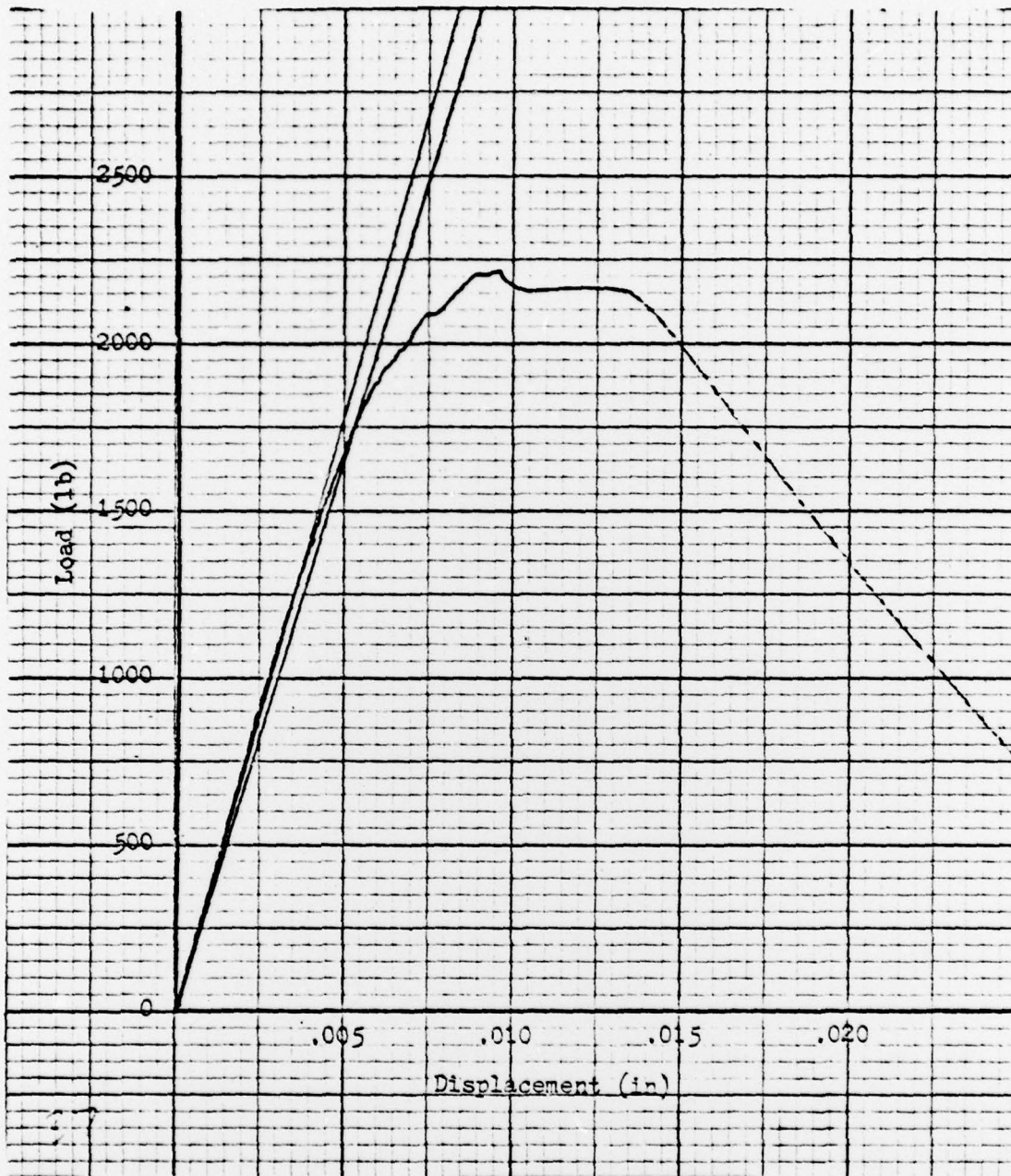


Fig. 27. Graph of 52100 UHC steel test three. This is a Type I record. The results were invalid for  $K_{IC}$ . Crack propagation consisted of a series of small steps.

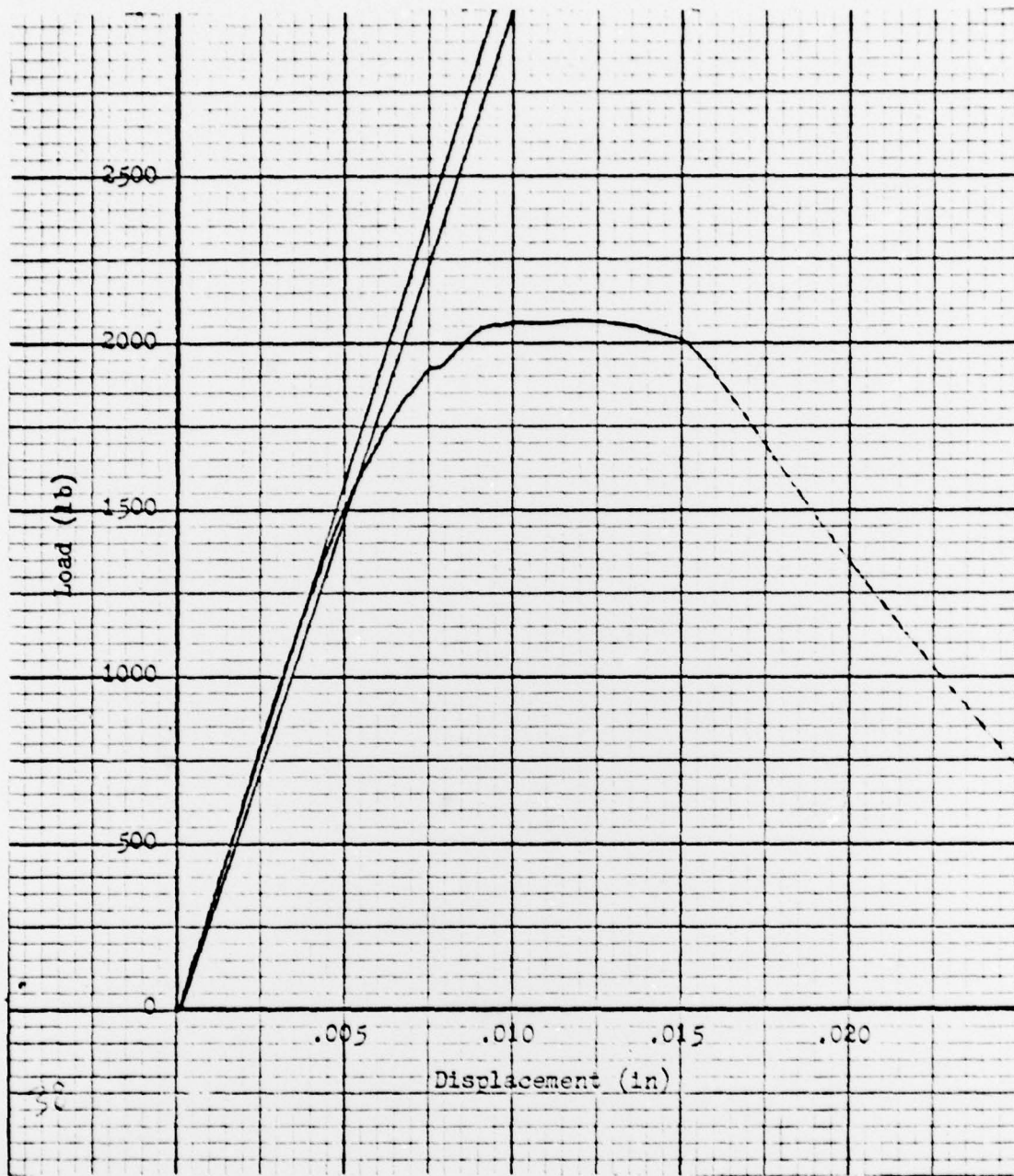


Fig. 28. Graph of 52100 UHC steel test four. This is a Type I record. The results were invalid for  $K_{IC}$ .

stopping cracks after small advances. The specimen strength ratio for this steel was 2.51, indicating that the material was over twice as tough as any other material tested, based on a comparison of these ratios. The variation in the apparent fracture toughness was 8.5% and the variation in the strength ratio results was 17.5%, based on four tests. For three of these tests the strength ratios were within 5.6% of each other.

#### 4. 52150 UHC Steel as Rolled

Tests were conducted on material from two heats of this steel. Tests on five specimens from the first heat did not allow determination of a valid  $K_{IC}$  due to several testing procedural problems. Examination of the surface of four of the specimens after fracture revealed that the fatigue precracks had not extended far enough into the specimen to meet the ASTM standard. The fatigue stress intensity factor for the remaining sample, as well as three of the other samples, exceeded 60% of  $K_Q$ . It was noted that the  $K_Q$  value for three of the tests had only a 10% scatter but the remaining two results varied widely from the average value. The apparent fracture toughness was calculated to be  $51 \text{ MPa}\cdot\text{m}^{1/2}$  and the specimen strength ratio was calculated to be 1.11, with a scatter of 19.9%.

Heat Two test results failed to produce a valid  $K_{IC}$  for much the same reasons as Heat One. Of the four tests conducted, only one result met the standard and the  $K_Q$  value of  $67 \text{ MPa}\cdot\text{m}^{1/2}$  from that test appeared much too high to be correct, based on all other test results for this material.

In any case, this value could not be accepted as valid since there was not a minimum of three successful tests. Two of the other three tests conducted failed because the fatigue stress intensity exceeded 60% of  $K_Q$ , and the remaining test failed because the ratio of  $P_{max}/P_Q$  exceeded 1.10. The average apparent fracture toughness was  $54 \text{ MPa}\cdot\text{m}^{1/2}$  and the strength ratio was 1.18 with a scatter of almost 50%. Insufficient test results were obtained to use the strength ratio with confidence.

#### 5. 10150 UHC Steel as Rolled

Although five tests were conducted on this material, a valid  $K_{IC}$  was not obtained for several reasons. The specimen minimum thickness requirement could not be determined because no tensile specimen was available to determine material yield strength. Thickness of test specimens was controlled by the available material thickness. On three of the five tests, the fatigue stress intensity exceeded 60% of  $K_Q$ . The apparent fracture toughness obtained from these three tests was  $59 \text{ MPa}\cdot\text{m}^{1/2}$  with a scatter of only 6%. The remaining two tests had  $P_{max}/P_Q$  ratios exceeding 1.10 and their  $K_Q$  results varied widely from those above. The apparent fracture toughness noted above was the second highest among those steels tested. This was not too surprising as the strength of this steel was lower than the other steels (comparing hardnesses) so toughness could be expected to be up somewhat. No specimen strength ratio could be calculated because the yield strength of the material was not known.

All graphs for this material were Type I records with no evidence of large pop-in crack propagation.

6. 10150 UHC Steel Annealed at 650°C

Tests were conducted on four specimens of this material heat treated with a one-hour anneal at 650°C and a subsequent air cool to room temperature. No valid  $K_{IC}$  could be determined because, again, the yield strength of this material was not determined as no tensile specimens were available. All four tests additionally failed to meet the ASTM standard as the fatigue stress intensity exceeded 60% of  $K_Q$ . The apparent fracture toughness of this material was calculated to be  $56 \text{ MPa}\cdot\text{m}^{1/2}$ , a reduction of 10% from the as-rolled condition. It was not possible to compare specimen strength ratios with the as-rolled material as these ratios could not be determined. There is no provision in the literature for comparing apparent fracture toughness values, so no conclusions can be drawn on the significance of this drop in  $K_Q$  in the annealed material, although it had been hoped that the anneal would improve this value.

7. 53150 UHC Steel Annealed at 650°C

Three specimens were tested after being annealed at 650°C for one hour and subsequently air cooled to room temperature. No valid  $K_{IC}$  could be determined since, again,  $K_f$  exceeded 60% of  $K_Q$ . In one of the tests the  $P_{\max}/P_Q$  ratio exceeded 1.10. The  $K_Q$  value for this material dropped 17% from the as-rolled  $K_Q$  value of  $42 \text{ MPa}\cdot\text{m}^{1/2}$ , with a scatter of 10%. No  $R_{sb}$  could be determined because no tensile test

specimens were available. Although no conclusions could be drawn from the drop in  $K_Q$  in the annealed material, it was not a response that had been anticipated.

Appendix A contains a table of specimen dimensions and a set of sample calculations for determining  $K_Q$  and  $R_{sb}$  for the reported 53150, 43150 and 52100 UHC steel test results.

#### IV. CONCLUSIONS

Based on the experimental observations and results, the following conclusions are made:

1. The Sherby Process has not achieved the fineness of microstructure for either spheroidal carbides or ferrite grains that had been anticipated. Since the option of further working the material is not available because of the minimum thicknesses required for ballistic testing, additional heat treatment or other processing should be considered to further refine the microstructure.

2. The steels containing fewer coarse carbides, the 52100 and 10150 UHC steels, performed better in fracture toughness testing than did the other steels. There was not sufficient data to conclude that the coarse carbides were the source of low toughness in these materials.

3. The UHC steels with higher carbon content were less tough than those with lower carbon content among those steels tested. It was hoped that the Sherby Process would provide higher carbon steels with better fracture toughness. Additional data is required on alloy steels in the 1.0 to 1.3 percent range before conclusions can be drawn as to the relationship between fracture toughness and carbon content for UHC steels.

4. Insufficient heat treatment data was generated to make conclusions on its effects on fracture toughness.

5. Increasing the width of the specimens may improve the control over fatigue precrack propagation and result in a higher percentage of valid tests.

6. Apparent fracture toughness results appeared insensitive to fatigue precrack stress intensities, which were as much as 15% over the standard maximum of 60% of  $K_Q$ .

7. Fracture toughness performance was poor for all UHC steels tested, with the exception of 52100 UHC steel. Ongoing study should place emphasis on this steel because of its availability, established manufacturing process and reasonable cost. This study should include examining various heat treatments and their ability to further refine the microstructure when combined with the Sherby Process. This material's combination of strength and toughness makes it a desirable alternative for many applications such as armor and bearing usage.

## APPENDIX A

TABLE VI

Specimen	Span S cm	Width W cm	Thickness B cm	Crack Length a cm
53150				
Test I	5.080	1.280	0.639	0.612
Test II	5.080	1.285	0.721	0.627
Test III	5.081	1.283	0.732	0.635
Test IV	5.080	1.283	0.721	0.635
43150				
Test I	5.081	1.275	0.693	0.584
Test II	5.081	1.275	0.693	0.686
Test III	5.080	1.275	0.693	0.622
Test IV	5.080	1.273	0.693	0.660
52100				
Test I	5.079	1.275	0.754	0.569
Test II	5.080	1.275	0.744	0.559
Test III	5.081	1.262	0.739	0.582
Test IV	5.080	1.270	0.744	0.622

## Sample Calculations:

## 52150 Test I Apparent Fracture Toughness

$$K_Q = \frac{P_Q \cdot S}{B \cdot W^{3/2}} \cdot f\left(\frac{a}{W}\right)$$

$$K_Q = \frac{(3.894 \text{ KN})(5.08 \text{ cm})}{(0.693 \text{ cm})(1.280 \text{ cm})^{3/2}} \cdot f\left(\frac{0.612 \text{ cm}}{1.280 \text{ cm}}\right)$$

$$K_Q = (19.71 \text{ MPa m}^{1/2})(2.49)$$

$$K_Q = 49 \text{ MPa m}^{1/2}$$

Reference 4 provides tabulated values for  $f\left(\frac{a}{W}\right)$  for the valid range of crack length/width ratios.

## Specimen Strength Ratio

$$R_{sb} = \frac{6 \cdot P_{\max} \cdot W}{B(W - a)^2 \sigma_{YS}}$$

$$R_{sb} = \frac{6(4272 \text{ N})(1.280 \text{ cm})(1 \text{ cm}^2)}{(0.721 \text{ cm})(1.280 \text{ cm} - 0.612 \text{ cm})^2 (951.4 \text{ MPa})(10^{-4} \text{ m}^2)}$$

$$R_{sb} = 1.02$$

#### LIST OF REFERENCES

1. Goesling, W. H., Ballistic Characterization of Ultra-High Carbon Steel, M.S. Thesis, Naval Postgraduate School, Monterey, California, 1977.
2. Rowe, D., and Hamilton, D. R., The Microstructural, Mechanical and Ballistic Characterization of Ultra-High Carbon Steel, M.S. Thesis, Naval Postgraduate School, 1977.
3. Martin, R. R. and Phillips, J. W., Ballistic Performance, Shear Band Formation and Mechanical Behavior of Thermo-Mechanically Processed Ultra-High Carbon Steel, M.S. Thesis, Naval Postgraduate School, 1978.
4. ASTM Committee E-24 on Fracture Testing, 1978 Annual Book of ASTM Standards, Part 10, American Society for Testing of Materials, 1978.
5. Third Semi-Annual Progress Report to Advanced Progress Research Agency under Grant DAHC-15-73-G15, Superplastic Ultra-High Carbon Steels, Stanford University Press, by O. D. Sherby and Others, February 1975.
6. Second Annual Report to Advanced Projects Research Agency under Grant DAHC-15-73-G15, Super Plastic Ultra-High Carbon Steels, Stanford University Press, by O. D. Sherby and B. Walser, August 1975.
7. Brick, R. M., Pense, A. W., and Gordon, R. B., Structures and Properties of Engineering Materials, 4th Edition, McGraw Hill, 1977.
8. Hillier, R., Evaluation of Superplastic Ultra-High Carbon Steel as Armor Plate for Critical Component Protection, M.S. Thesis, Naval Postgraduate School, Monterey, California, 1979.
9. Griffith, A. A., "The Phenomena of Rupture and Flow in Solids," Philosophical Transactions, Royal Society of London, Series A, Vol. 221, 1920.
10. Hayes, D. J., "Energy Balance Approach to Fracture," A General Introduction to Fracture Mechanics, Mechanical Engineering Publications Limited, 1978.
11. Irwin, G. R., "Fracture Dynamics," Fracturing of Metals, American Society of Metals, 1948.

12. Irwin, G. R., "Analysis of Stress and Strain Near the End of a Crack," Journal of Applied Mechanics, Vol. 24, 1957.
13. Orowan, E., "Energy Criteria for Fracture," Welding Research Supplement, 1955.
14. Hayes, D. J., "Stress Intensity Factor Approach of Fracture," A General Introduction to Fracture Mechanics, Mechanical Engineering Publications Limited, 1978.
15. Liu, H. W., "Fracture Toughness Testing and Its Applications," ASTM Special Technical Publication 381, 1965.
16. Rice, J. R., "A Path Independent Integral and the Approximate Analysis of Strain Concentration by Notches and Cracks," Journal of Applied Mechanics, June, 1968.
17. Turner, C. E., "Yielding Fracture Mechanics," A General Introduction to Fracture Mechanics, Mechanical Engineering Publications Limited, 1978.

INITIAL DISTRIBUTION LIST

	No. Copies
1. Defense Documentation Center Cameron Station Alexandria, Virginia 22314	2
2. Library, Code 0142 Naval Postgraduate School Monterey, California 93940	2
3. Department Chairman, Code 69Mx Department of Mechanical Engineering Naval Postgraduate School Monterey, California 93940	1
4. Associate Professor Terry R. McNelley, Code 69Mc Department of Mechanical Engineering Naval Postgraduate School Monterey, California 93940	6
5. LCDR James L. Taylor 10232 N.E. Beachcrest Drive Bainbridge Island, Washington 98110	1